UNCLASSIFIED

AD NUMBER
AD360456

CLASSIFICATION CHANGES
TO: **unclassified**
FROM: **secret**

LIMITATION CHANGES
TO: **Approved for public release, distribution unlimited**
FROM: **Distribution: Further dissemination only as directed by Director, Defense Atomic Support Agency, Washington, DC 20301, 05 MAY 1965, or higher DoD authority.**

AUTHORITY
DNA ltr dtd 6 Dec 1985; DNA ltr dtd 6 Dec 1985

THIS PAGE IS UNCLASSIFIED

SECRET
RESTRICTED DATA

AD **360456L**

DEFENSE DOCUMENTATION CENTER
FOR
SCIENTIFIC AND TECHNICAL INFORMATION
CAMERON STATION, ALEXANDRIA, VIRGINIA

Operation

SUN BEAM

This document consists of 125 pages

SHOT JOHNIE BOY

No. 172   of 237 copies, Series A

PROJECT OFFICERS REPORT—PROJECT 2.13

RADIOISOTOPE FRACTIONATION AND PARTICLE SIZE CHARACTERISTICS OF A LOW-YIELD SURFACE NUCLEAR DETONATION (U)

DDC

MAY 25 1965
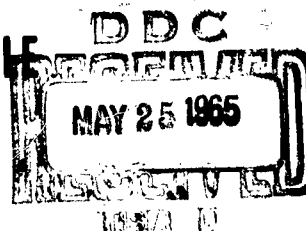
Irving J. Russell, Colonel, USAF,

Project Officer

Air Force Weapons Laboratory
Kirtland Air Force Base
New Mexico

| GROUP-1 |
| Excluded from automatic |
| downgrading and declassification. |

Issuance Date: May 5, 1965

RESTRICTED DATA

This document contains restricted data as
defined in the Atomic Energy Act of 1954.
Its transmittal or the disclosure of its
contents in any manner to an unauthorized
person is prohibited.

All distribution of this report is controlled.
Qualified DDC users shall request through
Director, Defense Atomic Support Agency,
Washington, D.C.   20301

DDC CONTROL
NO. 52184

SECRET

RESTRICTED DATA

Best Available Copy

Inquiries relative to this report may be made to

Director, Defense Atomic Support Agency
Washington, D. C.   20301

When no longer required, this document may be
destroyed in accordance with applicable security
regulations.

DO NOT RETURN THIS DOCUMENT

POR-2291
(WT-2291)

OPERATION SUN BEAM

SHOT JOHNIE BOY

PROJECT OFFICERS REPORT — PROJECT 2.13

RADIOISOTOPE FRACTIONATION AND PARTICLE
SIZE CHARACTERISTICS OF A LOW-YIELD
SURFACE NUCLEAR DETONATION (U)

*This document contains information affecting the Natio
Defense of the United States within the meaning of the
Espionage Laws, Title 18, U. S. C., Section 793 and 794
Its transmission or the revelation of its contents in t
manner to an unauthorzied person is prohibited by law.

Irving J. Russell, Colonel, USAF
Project Officer

All distribution of this report is controlled.
Qualified DDC users shall request through
Chief, Defense Atomic Support Agency,
Washington, D.C., 20301.

Air Force Weapons Laboratory
Kirtland Air Force Base
New Mexico

GROUP-1
Excluded from automatic
downgrading and declassification.

This document is the author(s) report to the Director,
Defense Atomic Support Agency, of the results of ex-
perimentation sponsored by that agency during nuclear
weapons effects testing. The results and findings in
this report are those of the author(s) and not neces-
sarily those of the DOD. Accordingly, reference to
this material must credit the author(s). This report
is the property of the Department of Defense and, as
such, may be reclassified or withdrawn from circula-
tion as appropriate by the Defense Atomic Support
Agency.

DEPARTMENT OF DEFENSE
WASHINGTON, D.C.   20301

3-4

ABSTRACT

Aircraft sampling penetrations of a low-yield nuclear cloud from a land-surface burst in Nevada were made at four altitudes, from 20 to 54 minutes after detonation. Samples from each of the four levels were radiochemically analyzed for 15 fission product isotopes. Other samples from each level were fractionated into seven particle size groups by settling in benzene. The individual size fractions were analyzed radiochemically and by gamma spectrometry. Particle size distributions and specific activities were measured in the untreated and artificially fractionated specimens of debris. Fallout samples were collected in trays along the fallout hot-line. The fallout samples were radiochemically and gamma spectrometrically analyzed.

The extensive radiochemical and physical data published by NRDL on the fallout samples (Reference 9) were used in conjunction with the cloud data to establish: (1) approximately 70 to 75 percent of Zr^{95} and the rare earth refractory fission products had fallen out of the cloud within 20 minutes of the detonation. Of the 25 percent remaining, about 15 percent later fell out locally and at intermediate distances; the remaining 10 percent resided in particles less than 18 micron diameter and was carried to larger distances. (2) Approximately 5 percent of Cs^{37} and Sr^{89} fell out of the cloud in the first 20 minutes. Of the Cs remaining in the 20-minute cloud, about 25 percent fell out locally and at intermediate distances; the remaining 70 to 75 percent was associated with particles less than 18 microns in diameter and was dispersed to larger distances.

The partitioning of 18 fission product chains between the cloud and the prompt fallout has been determined from the detailed radiochemistry of the cloud and fallout samples. All are intermediate between Zr and Cs in partitioning behavior.

The radiochemical composition of prompt fallout particulates can be systematized on the basis of a simple model employing the concept of fallout formation time.

The R value data for the cloud are satisfactorily fit by the relationship $R_{i,89} = (R_{95,89})^n$ where n varies between 0 and 1 for the different isotopes. The relationship is not extrapolatable to the composition of the fallout samples.

Three specific activity and particle size distribution behaviors can be discerned: irregulars in the cloud; irregulars in the prompt fallout; and spheres in the cloud.

The particle frequency functions for the irregulars in the cloud can be fit by $F(D) \propto /D^{3.2}$. The size distribution for spheres appears to be approximately lognormally distributed about a mean of 30 microns.

The specific activity of all isotopes in the cloud is highest in the smallest particles. S_{95} (fissions of Zr^{95} per gram) in the cloud decreases with increasing particle size but averages about 5×10^{13}, similar to the value in the most

intense prompt fallout samples. S_{137} in the cloud averaged 4×10^{14} fissions/gm compared to 1.2×10^{12} in the intense prompt fallout. The relationship between S_{95} and diameter is given by: $S_{95} \propto D^{-0.2 \pm 0.1}$. S^{137} follows no simple relationship with D over the entire size range but the distribution of Cs between particles $> 18\mu$ and $< 18\mu$ can be fit by $S_{137} \propto D^{-1}$. Data on the regulars (spheres) are tentative. The spheres exhibit a somewhat higher specific activity (S_{95}) than the irregulars. No more than 10 percent of the cloud fission activity is borne by spheres. Microprobe analysis demonstrates most spheres contain iron, with various quantities of Cr, Mn, Ni, and Zn, some of which show a tendency to be enriched relative to iron as particle size increases.

The importance of synthesizing data from cloud and surface sampling analysis programs is stressed. Isotopic fractionation is used as a tool in arriving at a partitioning between prompt and more remote fallout.

6

PREFACE

CONTENTS

9

SECRET

CHAPTER 1

INTRODUCTION

1.1 OBJECTIVES

The prime objective of this study was to define the radio-chemical and physical characteristics of the nuclear cloud in a three-dimensional sense and to relate these characteristics to those found in prompt fallout samples along the hot-line. Parameters to be investigated were: (1) the particle size distribution in the cloud; (2) the relationship between particle size and individual radionuclide specific activity of regular and irregular particles; (3) partition of isotope activity between the cloud and prompt fallout; (4) the ultimate disposition of the cloud's isotopic content downwind as determined by particle size considerations; (5) the fractionation systematics of the event; (6) the composition of regular and irregular particles as determined by electron beam microprobe analysis.

1.2 BACKGROUND

Only a handful of nuclear explosions have been conducted by the United States on continental land surfaces prior to Johnie Boy. These have all been of low yield (in the vicinity of 2 kt or less). Most have been the object of intensive fallout investigations since they represent the only basis on

GROUP 1
Excluded from automatic downgrading
and declassification

SECRET
RESTRICTED DATA

which to suggest similarity and differences between fallout phenomenology given by high-yield surface bursts on barges or on coral islands and the phenomenology that would result from high-yield continental surface bursts.

A sound fallout model leans heavily on assumptions concerning relationships between particle size and specific activity and the variation of these quantities with yield and burst conditions. Despite many years of experimental fallout studies much of the basic physical input data incorporated into fallout models and the scaling laws used in going from low to high yields are uncertain. Specifically open to question are (1) the particle size distribution, normally taken to be yield-insensitive and log-normal in form; (2) the relationship between specific activity and particle size, usually taken to be independent of particle size and unperturbed by fractionation; (3) the specific activity in a given size interval, commonly assumed to be directly scalable with yield; (4) the ignoring, until very recently, of the importance of isotope fractionation in affecting the character and intensity of the fallout field, and the partitioning between close-in and more remote fallout. Ideally, limitations of a fallout model should be imposed more by uncertainties in the meteorology and the three-dimensional distribution of the radioactive debris in the cloud than by inadequacies in basic physical data.

14

SECRET

The relatively poor understanding of close-in fallout phenomena (considering the large number of experimental opportunities provided) must be attributed in part to fragmentation of effort. Until recently only desultory attempts have been made to correlate information obtained from cloud samples with those derived from associated ground fallout samples. Traditionally, aerial cloud sampling and surface experimental groups had quite different objectives and borrowed little of each other's data. Notable contributions in recent years by Freiling (References 1 & 2) are in part due to a consideration of both cloud and ground fallout analyses. Also, useful information possessed by agencies that are not interested in the fallout problem per se can be extracted in a form that reveals no sensitive details. For example, if fission product R values of a given event are reported in terms of their ratio to an expected norm (the R value of an unfractionated sample appropriate to the device in question), then not even the fission product yield curve of the device is revealed. These normalized R values are referred to as R' in this report.

Isotopic fractionation is a powerful and relatively unexploited tool in the study of surface-burst explosions. If well documented spacially, isotopic fractionation patterns permit one to partition individual isotopic radioactivities

between persistent cloud components and fallout, and with
some confidence, between various particle fractions in the
persistent cloud.

   1.2.1 Characteristics of Ground-Burst Debris.
Stevenson (Reference 3), and Freiling (References 1 and 2)
have demonstrated the existence of systematic isotopic fractiona-
tion patterns in ground burst debris. The relevant data of
Stevenson and Freiling are mostly confined to large yield
Pacific coral island tests.

   Stevenson found that the fractionation patterns of cloud
samples from coral atoll surface shots can be reasonably well
fit by a linear R value plot. Freiling, however, in an
extensive study of the fractionation of coral island and
water surface bursts, in which cloud and fallout samples
both were measured, found it necessary to invoke a logarithmic
plot. Logarithmic plots of $R_{1,89}$ versus $R_{95,89}$ give straight
lines fitting both classes of burst quite well, under conditions
whereby R value ratios fractionated over a two order of magnitude
range.

   Freiling has suggested (Reference 2) that the power law
fit of the fractionated Sr^{89} R values, $R_{1,89} = (R_{95,89})^n$, may
be related to the mathematical fact that the product function x^n.
Log normal (x) is also log normal in form and with the same

16

variance. Thus, if the particle size distribution is log-normal, thé particle area and the particle volume functions should also be log-normally distributed. Freiling suggests that the most refractory isotopes, e.g., Zr^{95} and Ce^{144}, will be incorporated in the fallout material throughout the volume of the particles, whereas such species as Sr^{89} and Cs^{137}, which are mainly in the form of volatile precursors at the time of condensation of the particle matrix, will distribute themselves on the surface of the particles and will be log-normally distributed as D^2. All other radionuclide chains will exhibit an intermediate character between Sr^{89} and Zr^{95}, being partly attached to the surface and partly incorporated in the particle.

Since radionuclide composition and particle size are intimately related, with refractory isotopes showing an enrichment relative to volatile isotopes in large particles, at least the qualitative features of Freiling's hypothesis are borne out by the facts. It is possible, however, that a randomized surface attachment, directly related to the refractivity of the chain in question will probably equally well account for the observations. The closest approach to ideal condensation behavior, as Freiling emphasizes, should be given by airburst condensation processes, where the entire matrix is initially in the vaporized state. However,

17

the specific activity of individual airburst particles in the micron size range has been observed by the author to decrease with size. These airburst particles are highly enriched in refractory relative to volatile isotopes, and the majority of their activity is due to the refractory radioisotope components (Zr^{95} and rare earths). Hence one would expect a gross specific activity relationship which is essentially constant, or which falls off between D^2 and D^3. In fact, the fall off in specific activity with D is much steeper than D^2 in the majority of instances observed (Reference 4). In a surface burst a large fraction of the matrix to which the radioactive components can be attached has never been volatilized at all. Thus surface attachment of the fission fragments to larger inert particles must be considered an important mode of association in ground bursts.

Particle Size Distribution. The NRDL D-Model (Reference 5) for fallout assumes a log-normal particle size distribution for Nevada soil with $Log_{10}D = 2.053$ and $\sigma = 0.732$. Values adopted for coral are $log_{10}D = 2.209$ and $\sigma = 0.424$. RAND (Reference 5) uses a distribution defined by $log_{10}D = 1.65$ and $\sigma = 0.69$ to describe 95% of the cloud, and $log_{10}D = 2.34$ and $\sigma = 0.50$ to describe the remaining 5%. Both models

assume a uniform activity distribution with mass. For example, the RAND model with $\log_{10}D = 1.95$ puts 95% of the activity between 20 and 360 micron diameter particles, and with $\log_{10}D = 2.54$, 95% of the activity is between 160 and 1200 microns.

Specific Activity and Particle Size. The literature on particle size distributions, and specific activity as a function of particle size (mostly gross activity data, un-differentiated by nuclide assay), is abundant. This resume will confine itself to Jangle S, Jangle U, and Teapot ESS (References 6 through 8).

(1) The highest specific activities we have been able to find documented radiochemically for Jangle S and Jangle U are 2.9×10^{13} fissions of Mo^{99} per gram of fallout. In Jangle U, Mo^{99} appeared to be the most refractory isotope, judging from comparative analyses of Zr^{95} and Ce^{144} in the specimens (References 7 and 8). In Teapot ESS, S^{144} (expressed in fissions of Ce^{144} per gram of fallout and estimated by us from the dpm/gm data) exhibited a maximum of about 2.3×10^{13}, along the hot-line, although one sample collected 3,400 yards from ground zero gave an estimated S_{144} of 5×10^{14} fissions per gram (Reference 6). This is probably a sample of true fireball material. It is estimated that one ton of yield will vaporize about 0.4 ton of soil. Thus, a reasonable upper limit for

19

the specific activity of a soil-like fission product as
Ce^{144} would be about 3.5×10^{14} fissions/gm of prompt fallout.
The average specific activity for a given event is difficult
to determine without a comprehensive analysis of all pertinent
data. For example, in Teapot ESS, S_{144} increased from 4.5×10^{12}
at 300 yards (R/hr = 4150) to 2.3×10^{13} at 3,400 yards (R/hr = 43).
A crudely weighted average of about 5.5×10^{12} F_{144}/gm is
indicated.

(2) The specific activity generally decreased with particle
size but was constant to within a factor of two over the
range of 400 to 3000 microns. In Jangle S and Jangle U, 95% of
the total activity was found in particles in excess of 20
microns diameter. There is some tendency for enrichment of
Sr^{89} and Ba^{140} in the finer particles relative to Zr^{95} or
Ce^{144}. Typically, ground fallout particles contain less
than 10% of their representative Sr^{89} content and about 35%
of their representative Ba^{140} content relative to the refractory
isotopes   (Reference 6 through 8).

(3) The fraction of fully active particle in the
intense, prompt fallout increases with particle size. It
is estimated in Jangle U that 0.1%, 1%, and 10% of 1, 10, and
100-micron particles, respectively, were active. In Teapot ESS,
12% of particles larger than 200 microns were fully active
and 39% were surface active.

20

SECRET

(4) Hot particles have a number mean diameter larger than cold particles. The standard deviation of the frequency curves of hot and cold particles are comparable. The mass distribution for the prompt fallout along the hot-line generally is peaked to larger sizes than the undisturbed preshot soil.

(5) The radiochemical composition of cloud and fallout samples indicates severe fractionation of isotopic ratios of a complementary nature. The refractory isotopes Zr^{95}, Ce^{144}, and Mo^{99} are enriched in the fallout samples. The volatile isotopes Sr^{89}, Ba^{140}, Ag^{111}, and Ru^{106} are enriched in the cloud samples. To our knowledge material balance calculations have not been performed for these events, whereby an attempt was made to partition radioisotope activities between surface and the cloud.

CHAPTER 2

PROCEDURE

2.1 AIRCRAFT SAMPLING

Three WB-57 aircraft equipped with wing-tip tank samplers
penetrated the cloud at five levels between 20 and 54 minutes
after the detonation. Each tip tank exposed a 4.75-square
foot IPC filter paper. The tanks were equipped with an open-
close valve which was activated from within the aircraft. Flow
rate through the filter paper was approximately 1,500 linear
feet per minute. At these face velocities IPC was almost 100%
efficient for all particles with diameters in excess of ~.01
micron diameter. IPC is a cellulose mat paper which is
impregnated with kronisol (dibutoxyethylphthalate). Its
extreme purity from inorganic contaminants and its suitability
for dry or wet ashing manipulation in the laboratory render
it most useful for studying the chemical and physical properties
of aerosols.

The sampling aircraft were equipped with a number of
active and passive radiation measuring devices. Table 2.1
summarizes the salient features of each of the six independent
penetrations between 9,500 and 14,000 feet MSL, the approxi-
mate upper and lower boundaries of the intense cloud. Ground
zero was 5,153 feet MSL.

22

SECRET

In Table 2.1, R refers to roentgens and F to fissions.
F(gross) was obtained by Los Alamos between H + 1 and H + 2
hours, using standard assay techniques. F_{95} and F_{137}
were obtained radiochemically by assay of Zr^{95} and Cs^{137}.
The parenthesized numbers are exponents of 10, e.g.,
$1.6(14) = 1.6 \times 10^{14}$ (see **Appendix A**).

2.2 FALLOUT SAMPLING

Fallout samples were collected in 0.75 ft^2 cake pans
filled with Nevada soil, placed along the anticipated hot-
line (10° east of north) at 500, 700, 1,100, 1,300, and 1,500
yards from ground zero. The addition of soil to the pans
was most poorly conceived. The fallout samples were difficult
to analyze in a representative fashion, and only a limited
number of radiochemical and gamma spectrometric data were
obtained from them. They were useful, however, in demonstrating
some of the compositional relationships between the largest
debris found in the cloud and the fallout and provided
a few cross-check points on the very extensive radio-
chemical data on the fallout samples given in **Reference 9**.

23

2.3 AERIAL FILTER PAPER ANALYSIS

A portion of each filter paper was dissolved and analyzed radiochemically for Sr^{89}, Sr^{90}, Y^{91}, Zr^{95}, Mo^{99}, Cd^{115m}, Sn^{123}, Sn^{125}, Ru^{103}, Ru^{106}, Te^{129m}, Te^{132}, Cs^{137}, Ba^{140}, Ce^{141}, Ce^{144}, Pr^{143}, and Nd^{147}. Standard carrier radiochemical procedures were employed. The results are reported as R values. An R value is defined as:

$$R = \frac{(A_i/A_{99})_{J.B.}}{(A_i/A_{99})_{U^{235}}} \quad \text{(thermal fission)}$$

Here A_i is the disintegration rate of isotope i, A_{99} is the disintegration rate of Mo^{99}. The numerator is the disintegration rate of the isotope relative to Mo^{99} in Johnie Boy debris; the denominator is the ratio of the isotope disintegration

24

rate to Mo^{99} found in the thermal neutron fission of U^{235}. An R' value is defined in a similar fashion:

$$R = \frac{(A_1/A_{99})_{J.B.\ debris}}{(A_1/A_{99})_{J.B.\ unfractionated}}$$

The radiochemical analysis methods have been calibrated by thermal neutron irradiations and are generally accurate to about 10%.

2.4 PARTICLE SIZE AND SPECIFIC ACTIVITY STUDIES

2.4.1 Benzene Column Sedimentation. A known fraction of IPC filter paper was dry ashed at 450 to 500°C for 24 to 36 hours. The ash was suspended in benzene in a 500-ml graduated cylinder, vigorously stirred, and then allowed to settle for 120 minutes. The top 400 ml was withdrawn and filtered through Whatman #42 filter paper. (The filtrate was inactive). One quarter of the filter paper sample was reserved for microscopic particle sizing, as described below. The remainder was dissolved and transferred to an ampoule for gamma spectrometric measurements, using a 2- by 4-foot NaI well counter. The 100 ml of benzene suspension remaining contained all particles that had fallen

25

SECRET

from higher levels in 120 minutes. The volume was again made up to 500 ml with benzene, stirred, and then allowed to settle for 60 minutes. As before, the top 400 ml was withdrawn, filtered, and treated as above. This procedure was repeated for successive settling times of 30m, 15m, and 1m. The residue from the 1-minute settling fraction was filtered directly. In this manner, 28 samples (seven at each sampling level) were obtained for gamma spectrometry, radiochemical analysis, and optical microscopy.

2.4.2 Particle Sizing by Optical Microscopy. Particle size distributions were obtained on samples of unsized aerial filter samples and on those which had been subjected to the benzene column sedimentation. A few milligrams of the debris were suspended in a collodion-ether-alcohol solution, spread evenly on a glass microscope slide, and frequency-diameter data were recorded under magnifications of 100 to 500. The diameter recorded is the projection on the horizontal axis. Frequency curves were established for both irregular and for spherical particles (see Appendix B).

2.4.3 Gamma Spectrometry of Particle Fractions. Gamma spectrometric measurements were performed on the 28 benzene fractions, on samples of undifferentiated debris, and on soil samples. The majority of the measurements were performed 440

26

days or more after t_o. At this time, the samples contained only the following major γ-emitting components: $Ce^{144} - Pr^{144}$, $Ru^{106} - Rh^{106}$; $Zr^{95} - Nb^{95}$; Cs^{137}; and Co^{60}. Earlier measurements established the levels of $Ba^{140} - La^{140}$, Ce^{141} and Ru^{103} in selected samples. Interestingly, the late gamma spectra provide information on two very refractory isotopes (Zr^{95} and Ce^{144}), an isotope with intermediate volatility characteristics (Ru^{106}), an induced isotope (Co^{60}) and a very volatile isotope (Cs^{137}). Because of the limited number of components, and the reasonable separation of photo-peak energies, it was possible to establish the levels of all components to approximately 10%. The gamma spectrometric efficiencies were calibrated, post-facto, by radiochemical analysis of selected samples.

2.4.4 Specific Activity Measurements. Direct specific activity measurements were performed only on the 11K and 14K samples. Samples of dust were weighed and assayed on the gamma spectrometer. These represented the average specific activity, expressed in F_{95}, F_{144}, F_{137}, and F_{106} per gram. As well, each of the seven fractions obtained in the benzene sedimentation of the 11K and 14K debris were weighed and assayed. The specific activities of a few

27

individual particles of spherical debris were assayed on a
low background beta counter and the results expressed as
F_{144}/gm.

2.4.5 Electron Beam Microprobe Analysis. An Applied
Research electron microprobe analyzer was used in these
studies. Complete elemental analysis, within the limits
of the probe (Mg to higher Z), was performed on some two hundred
and fifty particles sampled from different heights. The
majority examined were metallic or metallic oxide spheres
in the 5 to 30 micron diameter range. Particles were located
and sized by the electron back-scatter technique. The probe
was switched to spot mode and an electron beam spot, one
micron in diameter, was positioned directly on top of the
particle in question. The X-ray detectors were then scanned
through the required wavelengths and the intensity versus wave-
length data were recorded as mass concentration units on
the read-out. Data are reported for Fe, Cr, Co, Ni, Mn,
Zn.   At the moment the unit has not been
calibrated for spherical particles of varying composition,
and the data reported are at best qualitative. Details are
to be found in Appendix D.

TABLE 2.1   CLOUD SAMPLING DATA (9500 to 14,000 feet MSL)

	9.5K	11K	11K	12K	13.5-14K	14K
A/C	842-R	842-L	842-L	245-L	245-R	827-L
Time	33 m	20 m	25 m	48 m	54 m	20 m
R/hr(ave)	4	10	30	0.05	4	75
R/hr(max)	6	60	60	0.1	8	200
t(sec)	30	10	15	68	83	17
R(total)	0.45	0.2	0.3	0.01	0.35	0.6
F(gross)	1.7(14)	4.2(14)	-	-	7.6(14)	8.4(14)
F/sec	0.57(13)	1.7(13)	-	-	0.9(13)	4.9(13)
F_{95}/sec	-	0.71(13)	-	-	-	1.0(13)
F_{137}/sec	-	1.6(13)	-	-	-	8.0(13)

CHAPTER 3

RESULTS AND DISCUSSION

3.1 DISTRIBUTION OF RADIOACTIVITY IN THE CLOUD

The active and passive radioactivity measurements summarized in Table 2.1 make it clear that the most intense portion of the cloud was in the vicinity of 14,000 feet, both at 20 and at 54 minutes after detonation. On any basis (peak R/hr, average R/hr, total fissions collected, or fissions per second collected), the intensity profile increases from the cloud bottom at about 9,500 feet to the top at 14,000 feet. The purpose to which the radiochemical data of the cloud will be put does not require a volume integration of the cloud but only a knowledge of its relative intensity as a function of altitude. In the sampling effort an attempt was made to penetrate the region of maximum intensity in each of the six passes. Accordingly we will adopt a profile of intensity versus altitude based upon the fission collection rate (F/sec) encountered at 9.5K, 11K, and 14K, from 20 to 33 minutes after t_o. The relative values are 1.0, 3.0, and 8.6 at three altitudes, respectively. These figures will be used to weight the radiochemical R values found at each of the four sampling altitudes in order to obtain an average radiochemical composition of the cloud. Table 3.1 gives the intensity versus altitude weighting factors adopted.

30

Although this procedure is quite arbitrary, the partition of
radioactivity between the cloud and the prompt fallout, which
will be derived from it, is relatively insensitive to the
weighting method adopted. Prime weight must be given, in
any event, to the 13.5 and 14-thousand foot samples.

3.2 RADIOCHEMICAL COMPOSITION OF CLOUD SAMPLES

The radiochemical R values, relative to Sr^{89}, are sum-
marized in Table 3.2 for the 9.5K, 11K, 13.5K, and 14K cloud
samples. The entry for Ave R will be explained in Paragraph
3.2.1.

In Figure 3.1 $R_{1,89}$ is plotted against $R_{95,89}$. The points
are seen to fit the relationship:

$$R_{1,89} = 1.00 \pm .05 \ (R_{89,95})^n$$

where n varies between 0 and 1. Species having the same
volatility characteristics in the cloud as Sr^{89} have zero
slopes on the log-log plot. Species having the same refractory
characteristics as Zr^{95} have slopes near 1.0. Those exhibiting
an intermediate behavior, as Ce^{141}, Y^{91}, Ba^{140}, Te^{129m} and
Te^{132} have intermediate slopes.

31

3.2.1 Average Composition of the Cloud.

Using the weighting factors in Table 3.1, the average value of the Sr^{89}/Zr^{95} R value ratio is calculated from the relationship:

$$\overline{R}_{89,95} = \frac{\sum W(Z) \cdot R(Z)}{\sum W(Z)}$$

$R(Z)$ was obtained from Table 3.2 by linear interpolation at 0.5K intervals. The result obtained is $\overline{R}_{89,95} = 3.43$, or $\overline{R}_{95,89} = .292$. To a good approximation, the average composition is given by the 13.5K cloud values in Table 3.2. Values chosen from the curves of Figure 3.1 at $R_{95,137} = .292$ are given in the final column of Table 3.2.

3.2.2 Radiochemical Composition and Particle Size.

The R values of Zr^{95}, Ce^{144}, and Ru^{106} relative to Cs^{137} for each of the 28 laboratory fractionated samples are given in Table 3.4. The data in Table 3.3 are based on gamma spectrometric measurements, supplemented by radiochemical analysis for calibration purposes.

In Table 3.3 the column headings refer to the time the debris was allowed to settle in the benzene column prior to decantation and filtration (see Section 2.4.1 for details). The approximate cut-off diameters of the particles, in microns for each of the seven fractions are listed in Table 3.4.

The cut-off diameters in the cloud have been estimated, assuming a cloud top of 15,000 feet, for several values of particle density, at the sampling times in question (Table 3.5).

Table 3.3 reveals a systematic fractionation of fission product R values with particle size. In general, there is a rough constancy in radiochemical composition between particles of 18 microns or smaller, although there is a tendency for Cs^{137} enrichment relative to Zr^{95} and Ce^{144} in the smallest particles, especially at the highest altitude. Particles in excess of 18 microns are highly enriched in Zr^{95} and Ce^{144} and to a less marked degree, in Ru^{106} all relative to Cs^{137}.

Figure 3.2 portrays the calculated particle size separations achieved by the benzene fractionation procedure. The figure gives the percent of particles of a given size in the original cloud sample for each of the seven settling times. These $\phi(D)$ functions, when multiplied by the particle size distribution characteristic of the cloud at time of sampling $(F(D))$, give the particle size distributions of each of the settled fractions, $F'(D)$. Thus,

$$F'(D) = \phi(D) \cdot F(D)$$

Use of the $\phi(D)$ functions will be discussed in Section 4.3.

3.2.3 Percentage Distribution of Radionuclides with Particle Size. In Table 3.6 are summarized the percentages of each of four radioisotopes in the 28 laboratory-fractionated samples. These data are relevant to the partition between short and longer term fallout of refractory, volatile and intermediate fission product isotopes.

33

3.3 PARTICLE SIZE DISTRIBUTION OF CLOUD SAMPLES

The gross particle size distribution of the cloud samples was determined in two independent manners by optical microscopy. Specimens of 11K and 14K debris obtained by ashing of the filter paper were sized directly. The curves obtained are illustrated in Figures 3.3 and 3.4, drawn through the circled points. The two curves are essentially superposable, as is to be expected if the cloud was initially well mixed, and the range of comparison is restricted to diameters below the cut-off values (72 and 137 microns, respectively). The size distribution function, $F(D)$, fits the data rather well over the range 2 to 60 microns with the form:

$$F(D) = K.D^{-2.95}$$

The second method involved sizing a portion of each of the seven fractions obtained by sedimentation in benzene. Only the 9.5K and 14K samples were treated in this manner. At each altitude, seven $F'(D)$ distributions were obtained. $\phi(D)$ values (Figure 3.2) appropriate to each settled fraction were applied to the $F'(D)$ distributions to obtain $F(D)$ over a portion of the particle size spectrum. The various segments of the distribution were spliced in over-lapping regions to give the curves drawn through the triangular points in

34

SECRET

Figures 3.3 and 3.4. The synthetic method gives a distribution
that can be reasonably well fit by:

$$F(D) = K.D^{-3.25}$$

3.3.1 Validity of Particle Sizing and Fractionation Methods.
With the exception of the larger number of smaller particles
observed below ten microns by the synthetic method, the two
approaches are in satisfactory agreement. There is a good
basis for preferring the form of the curve given by the
synthetic method at small diameters. The slopes of the
$F'(D)/\phi(D)$ curves obtained from the 120m, 60m, and 30m fractions
were significantly steeper than the slope observed in the
gross sample over the 1 to 18 micron range. In general, the
optical microscopy method, and the method used in dispersing
the particles for counting, tend to discriminate against the
smaller sizes when many large particles are present. The
low diameter cut-off fractions were free of this problem.
In any event, the mass or volume calculations are little
affected by a higher frequency of very small particles.
The area calculations are more sensitive to the form at lower
diameters however, and in Section 4.3 parametric adjustment
of the form of the active particle size distribution at low

35

diameters will be invoked to explain the particle size-radiochemical composition of the volatile isotopes.

Little if any fragmentation or agglomeration of the large particles appears to have occurred as a result of the vigorous stirring in benzene, judging from the similarity in the form of the distribution functions from 10 to 60 microns, as given by the undifferentiated and the benzene sedimented specimens.

The very high specific activity of the fine particles, and the marked difference in radiochemical composition between the fine and larger particles argue against attributing the steeper form of F(D) in the synthetic samples to fragmentation. (See Section 3.4 below, on specific activity considerations).

3.3.2 Size Distribution of Regulars and Spheres. Fewer than 1% of the observed particles could be identified as spheres or fused droplets. Because of the intrinsic interest in the spheres, the size distribution of the spheres was independently determined. The results are summarized graphically in Figure 3.5 where the percentage less than the stated size is plotted against the logarithm of the diameter. The distributions are approximately log normal in form, as predicted by Stewart (Reference 10) for the primary debris condensate, in contradistinction to the irregular particles in the cloud over the optical range. Table 3.7 gives the geometric mean diameter (D_g) and geometric standard deviation (σ_g) of the distributions.

The similarities between the 11K and 14K total samples may be noted. The smaller standard deviation of the 14K sample may be attributable to the lower cut-off diameter (72 versus 137 microns). In fact, the largest particles observed in the 14K and 11K samples, respectively, were 80 and 113 microns.

The form of the size distribution for the spheres can be described as:

$$F(D) = \frac{1}{(2\pi)^{1/2} \log \sigma_g} \exp\left(- \frac{(\log D_g - \log D)^2}{2 \log^2 \sigma_g}\right.$$

3.3.3 Modification of Cloud Distribution by Fallout.

Because of the time intervening between cloud stabilization (t_o) and sampling (t_s) the original particle size distribution $F(D)$ will have been modified by gravitational settling. Assuming a uniform distribution at t_o, and a cloud column of height H, measured from the cloud top, the fraction of particles of size D remaining in the column H after time t has elapsed is:

$$\phi = \frac{H - KD^2 t}{H}$$

The fraction falling out is $KD^2 t/H$ (Table 3.8). If the particle density is 2.5 g/cm^3, D is in microns, and a shape factor of 0.65 is used to allow for the modified fall rate of randomly shaped particles of effective diameter D, the constant K is 0.57 ft/hr for a unit diameter particle. Table 3.8 gives the fraction of particles of various sizes remaining in the cloud at $t_o + 20$ minutes, assuming the cloud top is 15K and the bottom is 9K.

37

While this is the hypothetical situation obtaining in the cloud
as a whole, the situation at a given altitude is somewhat simpler.
In a settling medium without turbulence, all particles of the
same size will fall with the same velocity. Thus, at a given
level the concentration of particles in all size groups will
remain constant if D is less than the cut-off value $D=(KH/t)^{1/2}$.
Above this size no particles of the original distribution
will be found. The approximate cut-off sizes given in
Table 3.5 were verified, in reasonable approximation, by
microscopic examination of the debris. A density of 2.5
gives a fair fit.

In this simplified picture, the radiochemical composition
differences between the 14K and 11K samples are those due
to the particle size fraction ranging from 72 to 137 microns.
The 9.5K and 11K samples, since they have similar cut-offs,
132 and 137 microns, should be quite similar in composition.
In fact, the 11K sample gives evidence of somewhat finer
debris. Interpretation of the sample obtained by penetrating
12K at H+48 and at 13.5-14K at H+54 is less clear cut. This
sample contains a higher percentage of volatiles than at 11K
but a smaller percentage than at 14K, despite the fact
that the cut-off at 13.5K is estimated to be 49 microns.
The assumptions of an initial uniform cloud, topping at 15K,
are of course, unsubstantiated by any direct data .

38

SECRET

3.4 SPECIFIC ACTIVITY OF CLOUD SAMPLES WITH PARTICLE SIZE.

Specific activities (S_i), expressed as isotope fissions per gram of particulate fallout, were obtained in separate benzene sedimentation experiments, using the 11K and 14K samples. Disagreements between the internal radiochemical composition of Table 3.9 with those in Tables 3.3 and 3.6 reflect the failure of the two independent settling experiments to yield completely reproducible results.

A few spheres were isolated in the 46 to 101-micron size range and counted on the low beta background system. The S_{144} values observed ranged from 1.5 x 10^{14} F_{144}/gm to 6.5 x 10^{14} F_{144}/gm. The fission product activity in these particles, measured about two years after t_o, was predominately Ce^{144}. The range of specific activities quoted above was based on the hard component of the Ce^{144}-Pr^{144} beta absorption curve. Further work is needed to confirm the radioactive content of these microspheres. The very high F_{144}/gm is 3 to 10 times that found in other cloud and fallout samples and calls for verification.

3.5 SPECIFIC ACTIVITY OF GROUND FALLOUT SAMPLES

3.5.1 NRDL Measurements.

A very extensive set of radio-chemically determined specific activities is reported in Reference 9. The most relevant are those measured in the fallout along the hot-line. Lower specific activity samples are generally found off the hot-line and are likely to represent higher admixtures of inert throw-out. The data summarized in Table 3.10 represent, in our judgment, the specific activity of the bulk of the prompt fallout, expressed in equivalent fissions per gram of Zr^{95}, Sr^{89}, Sr^{90}, and Y^{91}. The columns are: NRDL sample number, distance, fissions per square foot, and S_i. Parenthesized numbers are powers of ten.

In comparing these average numbers with the cloud values in Table 3.9, the S_{89} values can be considered roughly equivalent to the S_{137} (Sr^{89} and Cs^{137} are about equally volatile). Ru^{106} has a volatility character similar to Sr^{90}. It is to be noted that there is little difference between S_{95} in the 14K cloud and the fallout samples, whereas the Cs^{137} specific activity in the cloud is about 170 times higher than its equivalent, Sr^{89}, in the fallout (Sr^{89}/Cs^{137} in prompt fallout ~1).

3.5.2 Average Specific Activity and Particle Size.

Reference 9 reports a large volume of data on the relationship of specific activity and particle size. In Table 3.11 we tabulate the approximate values of the median mass diameter

and the median activity diameter of a set of fallout samples.
Asterisked samples refer to those along the hot-line. The
values were obtained from Table 3.4 of **Reference 9** by inter-
polating to obtain the approximate diameter representing 50%
of the cumulative mass or activity.

In general, the activity distribution was peaked toward the
larger particles. Station 11A07 experienced the heaviest
fallout, and the distribution was apparently more uniform in
samples along the hot-line. The preshot soil sample had a
median mass diameter of about 124 microns (Reference 9).

In the prompt fallout there is not a strong correlation
between radiochemical composition and particle size, although
there is a slight tendency for enrichment of volatile isotopes
relative to refractories in the less than 44 micron fraction
(See Table 3.15, Reference 9).

3.5.3 Specific Activity of Fused Agglomerates. We have
determined F_{144}/gm of 24 lava particles taken along the hot-
line between 1,500 and 4,500 feet. These particles were in the
500 to 1,200 micron interval. Their description ranged from
spheres to pellets and irregular lava-like masses. The
average value of S_{144} obtained was 1.88×10^{14}.
S_{144}/S_{137} varied systematically from 700 to 1,500 yards, increasing
by a factor of 1.65 over this distance.

41

The average S_{144} of these fused masses is about 3.3 times higher than S_{95} (and therefore, S_{144}) reported in Table 3.10 and represents a very efficient incorporation of refractory fission products into volatilized or fused soil.

3.5.4 Radiochemical Composition of Ground Fallout. As in the case of the cloud samples an estimate will be made of the average radiochemical composition of the prompt fallout. Data for Zr^{95}, Sr^{89}, Sr^{90}, and Y^{91} were taken from Table 3.10 and represent the weighted averages found along the hot-line. The average of 11 Ce^{144}/Zr^{95} and Mo^{99}/Zr^{95} samples in the prompt fallout showed a standard deviation of less than 10%

and was, within the standard deviation, equal to values reported in Reference 9 for the cloud samples. Hence it appears that Mo^{99} and Ce^{144} as reported by Tracerlab are systematically high with respect to Zr^{95} by factors of 1.15 and 1.22 respectively. In Table 3.1, cloud R values for Mo^{99}, Zr^{95}, and Ce^{144} are all very close to 1.00. Material balance does not permit Mo^{99}/Zr^{95} values in excess of 1 in both cloud and prompt fallout samples. Accordingly, in the final tabulation to follow, in the interest of consistency we have reduced the Zr^{95} ratios by a factor of 1.15, in the prompt fallout.

Most of the analyses for other isotopes reported in Tables 3.14, 3.15, and 3.16 of Reference 9 were performed on samples somewhat off the hot-line. To estimate the values in the hot-line samples of such species as I^{131}, Te^{132}, Cs^{136}, Cs^{137}, Ba^{140}, and Ce^{141}, $R_{1,95}$ were plotted against $R_{89,95}$, and values were selected for $R_{1,95}$ when $R_{89,95}$ = .0317, the weighted hot-line value for Sr^{89}/Zr^{95}. Cs^{137}, Ru^{103}, and Ru^{106} were taken as the average of the three O1AO7 samples, normalized to Sr^{89}/Zr^{95} = .0317. The R value plots appear in Figures 3.6a and 3.6b, and the selected values for the weighted isotopic content of the prompt fallout with respect to Zr^{95} are given in Table 3.12.

R values have been estimated also for $R_{89,95}$ = .1 from the fractionation plots (Figures 3.6a and 3.6b). These R values will be used in Section 4.2 to describe the fallout composition between 6 and 20 minutes.

TABLE 3.1 INTENSITY PROFILE IN CLOUD

Altitude (Kft)	Intensity
9.5	1.00
10.0	1.53
10.5	2.15
11.0	2.99
11.5	3.69
12.0	4.47
12.5	5.26
13.0	6.30
13.5	7.19
14.0	8.62

TABLE 3.2 R VALUE SUMMARY OF CLOUD RELATIVE TO Sr^{89}

	9.5K	11K	13.5K	14K	Ave R
Sr^{90}	0.97	0.95	0.96	1.00	0.97
Y^{91}	0.89	0.75	0.66	0.61	0.70
Zr^{95}	0.64	0.53	0.28	0.173	0.292
Mo^{99}	0.65	0.51	0.29	0.167	0.29
Sn^{125}	1.02	1.01	0.93	0.89	0.92
Te^{129m}	0.95	0.91	0.98	0.76	0.82
Te^{132}	0.91	0.91	1.07	0.81	0.86
Cs^{137}	1.02	1.01	1.08	1.07	1.05
Ba^{140}	0.88	0.87	0.82	0.66	0.77
Ce^{141}	0.99	0.79	0.63	0.48	0.62
Pr^{143}	0.58	0.42	0.30	0.178	0.29
Ce^{144}	0.62	0.52	0.23	0.170	0.29
Nd^{147}	0.59	0.42	0.24	0.154	0.26

TABLE 3.3   RADIOCHEMICAL COMPOSITION AND PARTICLE SIZE

$$R_{95,137}$$

	Res	1m	5m	15m	30m	60m	120m
9.5K	3.4	0.62	0.46	0.32	0.26	0.23	0.19
11K	2.5	0.59	0.31	0.24	0.20	0.20	0.19
13.5K	0.78	0.45	0.20	0.16	0.13	0.14	0.12
14K	1.3	0.26	0.24	0.11	0.095	0.084	0.073

$$R_{144,137}$$

	Res	1m	5m	15m	30m	60m	120m
9.5K	3.4	0.66	0.39	0.27	0.23	0.22	0.20
11K	2.5	0.61	0.31	0.23	0.21	0.21	0.17
13.5K	0.84	0.45	0.18	0.15	0.13	0.12	0.12
14K	1.2	0.32	0.21	0.084	0.11	0.089	0.081

$$R_{106,137}$$

	Res	1m	5m	15m	30m	60m	120m
9.5K	1.5	1.4	0.78	0.79	0.59	0.64	0.49
11K	1.5	0.97	0.90	0.51	0.57	0.60	0.54
13.5K	1.0	0.95	0.58	0.85	0.52	0.66	0.70
14K	1.8	0.94	0.79	0.65	0.79	0.57	0.59

TABLE 3.4 CUT-OFF DIAMETERS IN MICRONS

Res	1m	5m	15m	30m	60m	120m
137*	67	31	18	12.8	9.0	6.4

*The residue contained all particles greater than 67 microns. The cut-off is determined by the largest particle that should have been in the cloud at time of sampling.

TABLE 3.5 CUT-OFF DIAMETERS IN CLOUD

	9.5K	11K	13.5K	14K
Time	33m	23m	54m	20m
ρ = 1.50	171	176	64	94
ρ = 2.00	148	153	55	81
ρ = 2.50	132	137	49	72

TABLE 3.6 PERCENTAGE DISTRIBUTION OF RADIONUCLIDES WITH SIZE

	Res	1m	5m	9.5K 15m	30m	60m	120m
Ce^{144}	63.5	4.9	3.3	4.3	7.4	11.0	5.7
Zr^{95}	61.4	4.5	3.9	4.9	8.2	11.6	5.5
Cs^{137}	11.4	4.6	5.2	9.7	19.7	31.1	18.6
Ru^{106}	21.2	8.8	5.5	10.3	15.5	26.4	12.3

				11K			
Ce^{144}	55.6	11.3	6.1	7.3	7.3	9.0	3.6
Zr^{95}	56.7	10.8	6.1	7.5	6.7	8.7	4.0
Cs^{137}	11.8	9.7	10.2	16.6	17.9	22.3	11.3
Ru^{106}	24.4	12.7	12.4	11.2	13.5	17.8	8.1

				13.5K			
Ce^{144}	36.9	24.9	6.5	7.4	7.4	10.5	6.4
Zr^{95}	33.9	24.8	7.4	7.7	7.7	12.0	6.7
Cs^{137}	11.3	14.4	9.6	12.9	15.1	22.5	14.2
Ru^{106}	15.3	18.4	7.5	14.8	10.6	20.0	13.4

				14K			
Ce^{144}	40.3	6.7	6.8	6.6	17.0	17.0	4.4
Zr^{95}	42.6	5.6	6.8	6.6	17.0	17.0	4.4
Cs^{137}	5.6	3.6	4.8	10.7	30.5	34.6	10.3
Ru^{106}	13.8	4.6	5.1	9.3	32.5	26.4	8.2

TABLE 3.7 SIZE DISTRIBUTION OF SPHERES

	1.1K (Total)	1.4K (Total)	9.5K (Residue)	1.4K (1 Min)	1.4K (Residue)
D_g	33.5	33.5	51	11	46
σ_g	1.87	1.45	1.41	1.70	1.39

TABLE 3.8 FRACTION OF PARTICLES LOST BY FALLOUT

	5%	10%	20%	30%	40%	50%
μ	59	35	78	95	110	123

	60%	70%	80%	90%	100%
μ	134	149	156	165	176

TABLE 3.9   SPECIFIC ACTIVITY OF CLOUD FRACTIONS

Fraction	11000 Foot			14000 Foot		
	S_{95}	S_{106}	S_{137}	S_{95}	S_{106}	S_{137}
120m	8.1(13)	1.6(14)	2.9(14)	5.1(13)	3.2(14)	4.1(14)
60m	7.9(13)	1.9(14)	3.1(14)	9.1(13)	2.8(14)	7.3(14)
30m	5.8(13)	1.2(14)	2.1(14)	8.8(13)	2.9(14)	7.0(14)
15m	4.4(13)	9.1(13)	1.6(14)	7.3(13)	2.2(14)	5.7(14)
5m	3.4(13)	5.5(13)	9.5(13)	5.1(13)	2.3(14)	3.9(14)
1m	3.2(13)	2.7(13)	4.0(13)	3.9(13)	9.4(13)	2.2(14)
Residue	3.7(13)	2.1(13)	2.3(13)	4.2(13)	5.1(13)	1.1(14)
Ave.	4.1(13)	5.0(13)	7.9(13)	5.5(13)	1.3(14)	3.4(14)

In the above table the parenthesized numbers are powers of ten.

TABLE 3.10   SPECIFIC ACTIVITY OF GROUND FALLOUT

Sample	Distance	F/ft^2	S_{95}	S_{89}	S_{90}	S_{91}
01A07	1200 ft	7.9(13)	6.1(13)	1.8(12)	5.8(12)	1.9(13)
11A07-#4	1342 ft	6.5(15)	5.3(13)	1.9(12)	6.5(12)	3.1(13)
21A03-4	2830 ft	2.7(15)	6.4(13)	2.4(12)	8.3(12)	3.8(13)
31A03	4717 ft	4.5(14)	7.9(13)	3.1(12)	9.0(12)	5.2(13)
Average, weighted by F/ft^2			5.7(13)	2.1(12)	7.0(12)	3.4(13)

TABLE 3.11   MEDIAN MASS AND MEDIAN ACTIVITY DIAMETERS

Sample	MMD(microns)	MAD(microns)	Distance
01A02	220	1400	1200 ft
01A03	310	1950	1200 ft
01A05	350	1450	1200 ft
02A04	177	1050	1200 ft
*11A07-2	>1000	>1000	1342 ft
12A079	210	1550	1342 ft
20A04	67	2830	2400 ft
20A07	250	1000	2400 ft
*21A0-1	-	1400	2830 ft
30A01-8	70	1250	4000 ft
*31A05	710	750	4717 ft
*32A08	610	750	4717 ft
*31A05-8	710	810	4717 ft

TABLE 3.12   RADIOCHEMICAL COMPOSITION OF PROMPT FALLOUT

Zr^{95} R' Values

	0-6m	6-20m		0-6m	6-20m
Sr^{89}	0.0317	0.100	I^{131}	0.083	0.95
Sr^{90}	0.107	0.40	Te^{132}	0.061	0.59
Y^{91}	0.512	0.82	$*Cs^{136}$	0.49	-
Mo^{99}	1.00	1.00	Cs^{137}	0.034	0.35
Zr^{95}	1.00	1.00	Ba^{140}	0.28	0.67
Ru^{103}	0.74	0.95	Ce^{141}	$0.46 \pm .15$	0.83
$*Ru^{106}$	0.08	0.40	Ce^{144}	1.06	1.00

In the above table, asterisked values have been divided by 1.6
to normalize for their increased yield in bomb spectrum fission.
The values in the table for Sr^{89}/Zr^{95} = .0317 are estimated to
be good to 10% for Sr^{89}, Sr^{90}, Y^{91}, Mo^{99}, Zr^{95}, Ba^{140}, and Ce^{144}
and to $\pm$ 25% of the quoted value for the remaining isotopes,
unless noted. The values for Sr^{89}/Zr^{95} = 0.1 are considerably
less well established and are based exclusively on the lines
drawn through the data points of Figures 3.6a and 3.6b.
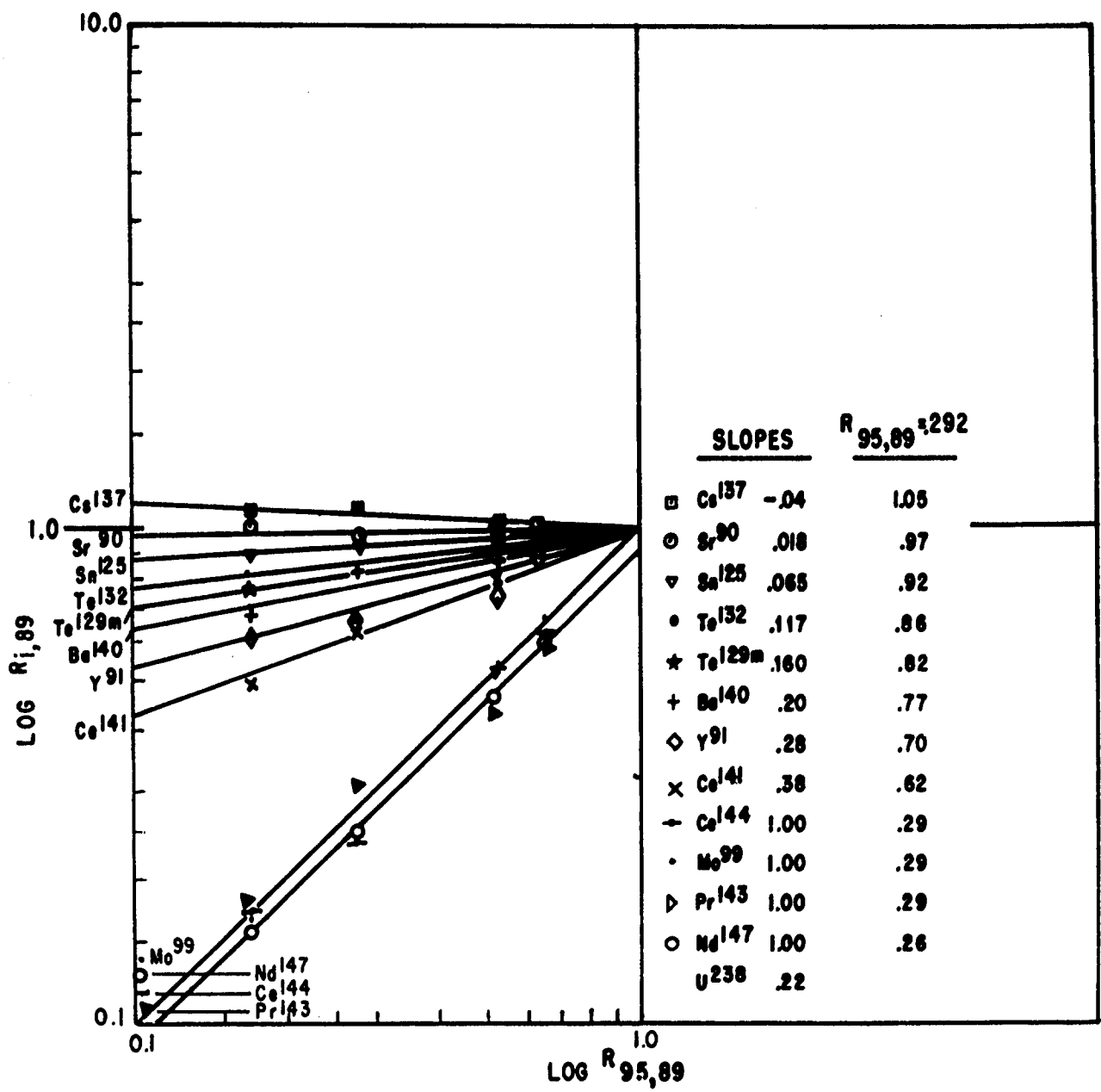
Figure 3.1 Fractionation plots cloud samples.
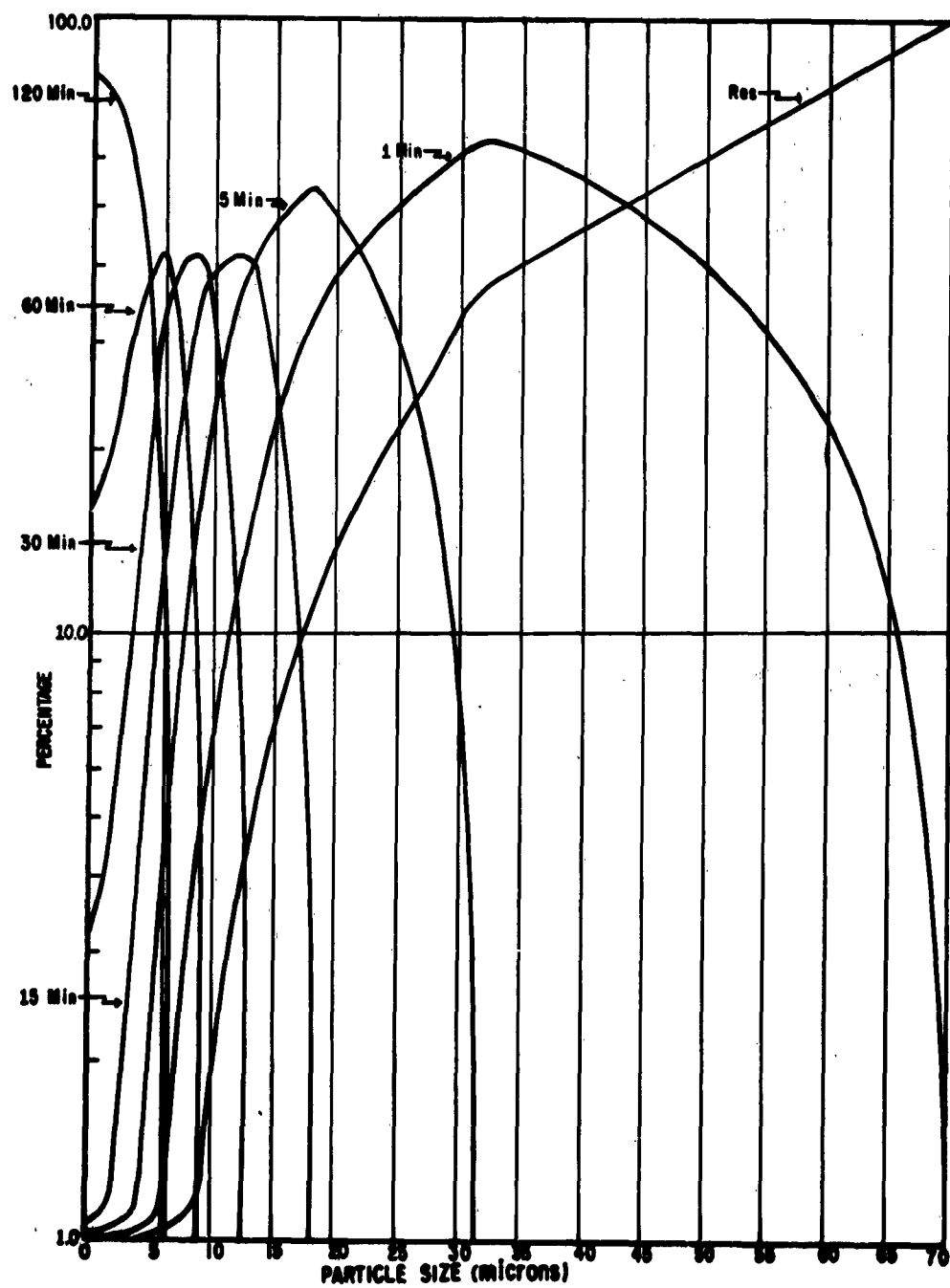
Figure 3.2   Benzene fractionations.

53

SECRET
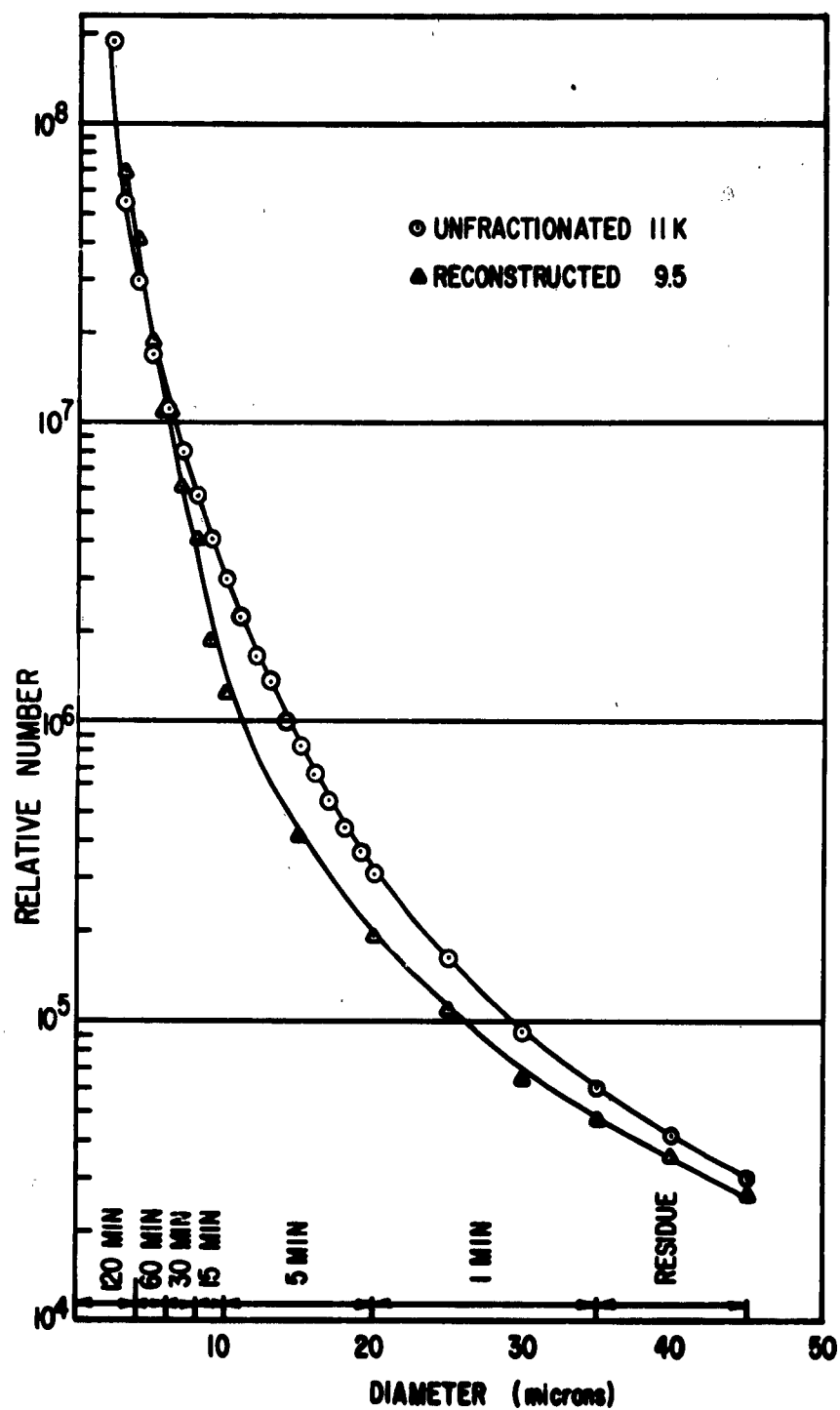
Figure 3.3 Particle size distribution.
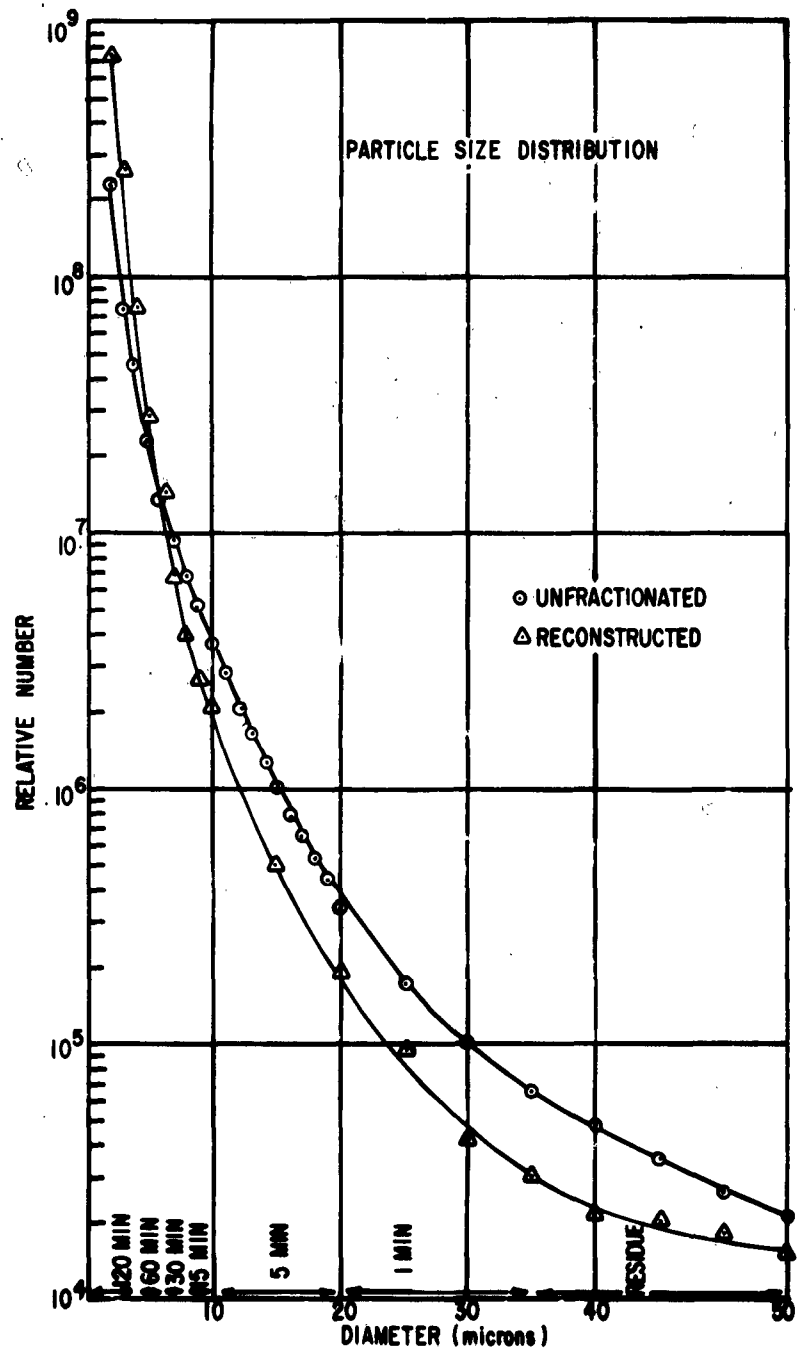
Figure 3.4   Slope reconstruction, 14k feet.

55

SECRET
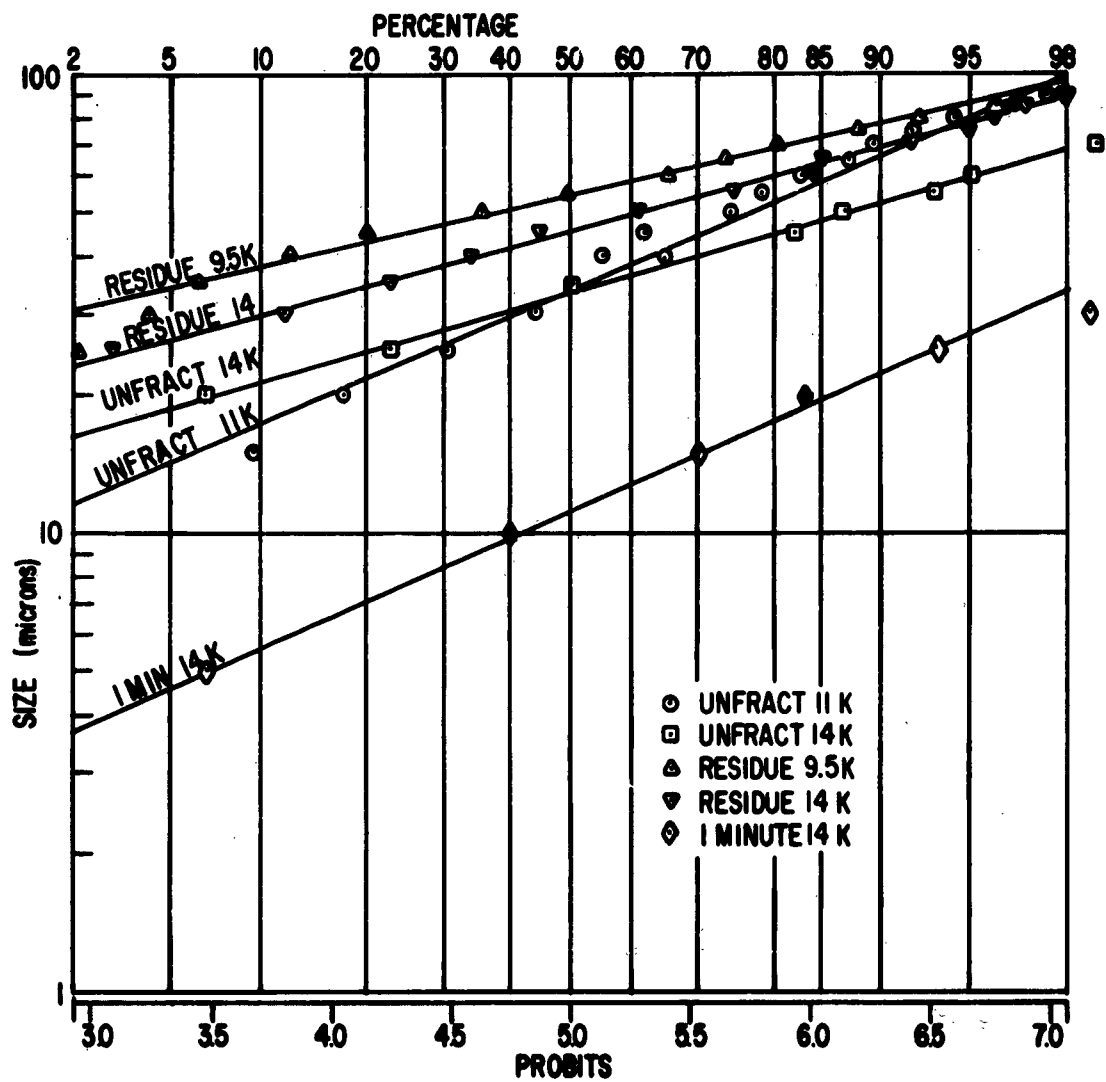
Figure 3.5 Sphere distribution.
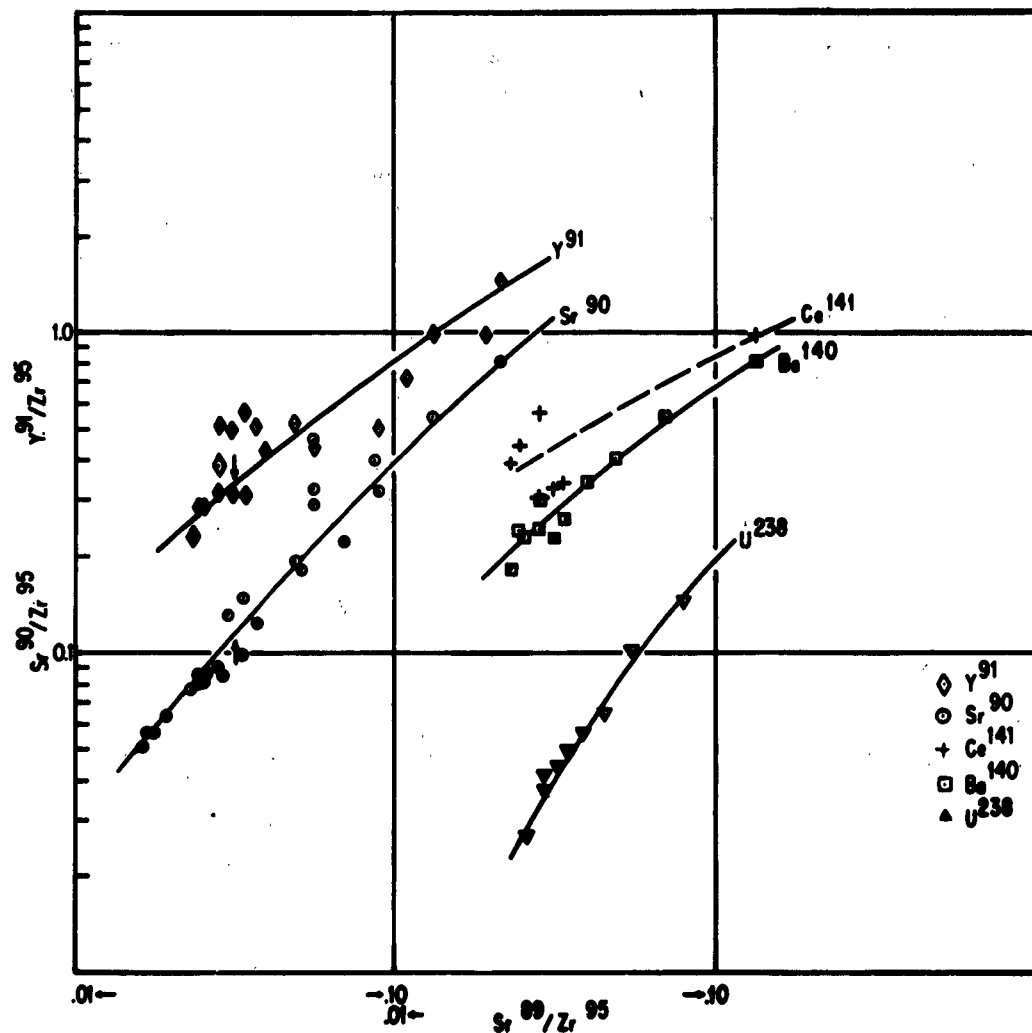
Figure 3.6a   Fractionation plots, fallout samples.

57
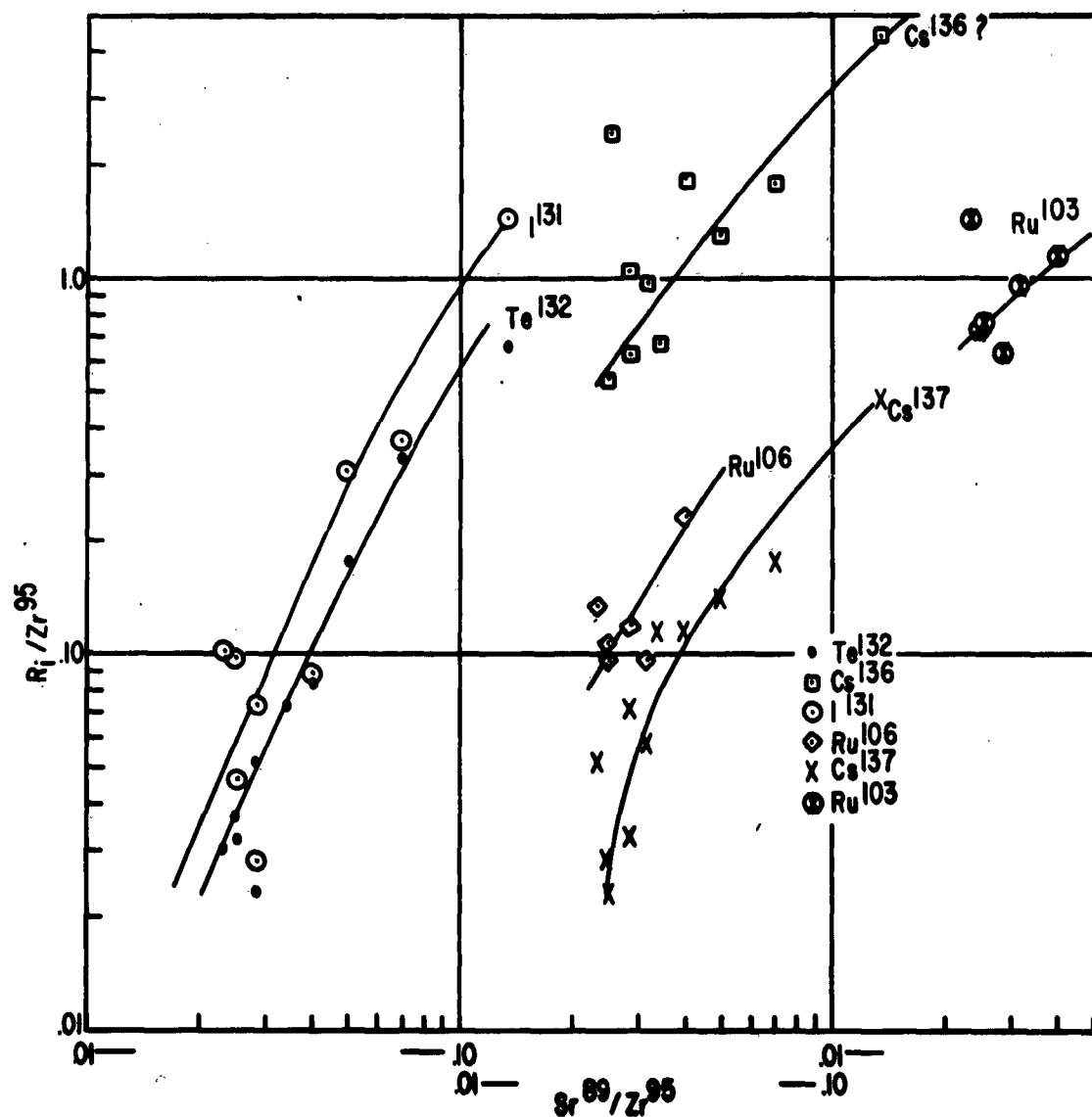
Figure 3.6b Fractionation plots, fallout samples.

CHAPTER 4

INTERPRETATION OF DATA

4.1 FALLOUT FORMATION TIME AND RADIOCHEMICAL COMPOSITION

A provisional attempt has been made to interpret the fallout sample fractionation plots of the alkaline earths and Ce^{141}. The Bolles-Ballou fission chain populations as a function of time since fission (Reference 12) (or adjusted values thereof based on revised half lives) were multiplied by a set of relative attachment coefficients for the several precursor fission elements. $R_{i,95}$ were then calculated versus time and calculated $R_{i,95}$ values were plotted against the associated $R_{89,95}$ numbers. The attachment coefficients (k_i) were chosen to give a consistent and physically reasonable fit to the experimental data. In this very simple model the k_i were assumed to be time independent. k_{Kr}, k_{Xe}, k_{Br} and k_I were taken to be 0, although there is evidence from Cs^{137} R value data that $k_I > 0$. k_{Sr}, k_Y, k_{Zr} and k_{Ba} were all taken to be 1.00. The observed fit was obtained by using $k_{Rb} = 0.22$ and $k_{Cs} = 0.15$. In principle, $R_{136,95}$ should be used for k_{Cs}, since Cs^{136} is independently formed in fission. However, the Cs^{136} data do not meet the mass balance criterion for cloud and fallout samples and are suspected of being too high.

The experimental $R_{1,95}$ values deducible from the data reported in Tables 3.15 and 3.16 of Reference 9 were plotted against the appropriate values of $R_{89,95}$. A comparison of the calculated and the experimental data is shown in Figure 4.1. The systematization achieved is satisfactory considering the gross simplicity of our assumptions. The results suggest that the time required to form a segment of the fallout cloud may be equally relevant to the interpretation of fallout plots as is the concept of surface versus volume incorporation.

One anomaly deserves mention. The excellent fit given by Y^{91} in Figure 4.1 holds only for samples off the fallout hot-line. Samples 11, 21, and 31 along the hot-line had Y^{91}/Zr^{95} ratios approximately 1.5 times higher than expected for the associated Sr^{89}/Zr^{95} and Sr^{90}/Zr^{95} values. The fallout required 1.5 m, 3.3 m, and 6 m, respectively to reach the ground at 1342, 2830, and 4717 feet from ground zero (Reference 9). As the particles proceed downwind, the proportion of Rb and Sr in the vapor phase increases, and surface attachment should thereby be favored for particles still in contact with the vapor. However, to explain the Sr^{89} and Sr^{90} ratios to Zr^{95} in these samples it must be assumed that k_{Sr} increases with respect to k_{Rb} as the cloud passes downwind. A subsequent addendum to this report will attempt to treat these and the remaining isotope data in a more quantitative fashion.

4.2 PARTITION OF ISOTOPE ACTIVITY BETWEEN CLOUD AND FALLOUT

Applying the constraint that $R_{1,95} = 1.00$ for all fission product isotopes as formed, it follows that:

$$\frac{F_{95}(\text{fallout})}{F_{95}(\text{cloud})} \qquad \frac{\overline{R}_{1,95}(\text{cloud}) - 1}{1 - \overline{R}_{1,95}(\text{fallout})}$$

Two extreme isotopes, Sr^{89} and Zr^{95}, form the basis of the partition calculation. $\overline{R}_{89,95}(\text{cloud})$ has been established as 3.43 (see Table 3.2). The value of $\overline{R}_{89,95}(\text{fallout})$ remains to be determined.

The average radiochemical composition of the prompt fallout given in Table 3.12 pertains to the material that had fallen on the ground within six minutes. The Sr^{89}/Zr^{95} of this component is 0.0317. An analysis of the fallout contours reported in Reference 11 suggests that approximately 25 percent of the fallout occurring between 0 to 20 minutes took place between 6 to 20 minutes. Thus, the appropriate value of $\overline{R}_{89,95}(\text{fallout})$ to use in the above equation is:

$$\overline{R}_{89,95}(\text{Fallout}) = 0.75 \times 0.032 + 0.25(R_{89,95}, \text{ 6 to 20 min})$$

Unfortunately we have no direct measurements to suggest the value of $R_{89,95}$ in the 6 to 20 minute fallout. However, the bulk of the fallout in this interval was in the 150 to 400 micron size range. The data reported in Reference 9 give no evidence that

61

material in this size range along the hot-line is significantly different in composition from the larger particles representing the bulk of the deposited mass. An upper limit of $R_{89,95} = 0.3$ can be established with reference to the composition of the residue fraction found at 9.5K 33 minutes after t_o (Table 3.3). On this basis, $F_{95}(\text{fallout})/F_{95}(\text{cloud}) = 2.72$, as opposed to 2.50, obtained when $R_{89,95} = 0.0317$ is used. Thus, the result is insensitive to $R_{89,95}$ (fallout) and for either situation the fraction of Zr^{95} in the fallout is $72\pm1\%$. However, the Sr^{89} in the fallout for these two cases is changed from 7.4% to 2.3%.

These differences will affect only to a small degree the calculated partition of all other isotopes if the set of cloud analyses is used for the calculation. The average R_{89} values are given in Table 3.2 for the cloud samples. The percentage of any isotope remaining in the cloud is merely:

$$\%_i \text{ (Cloud)} = \bar{R}_{i,89} \times \% \, Sr^{89} \text{ (Cloud)}$$

If the set of fallout analyses is used to calculate the partition, the result is very sensitive to the choice of Sr^{89}/Zr^{95} in the 6 to 20-minute fraction of the fallout. This arises because of the steep slopes of the fractionation plots (Figures 3.6a and 3.6b). A trial calculation indicates that Sr^{89}/Zr^{95} of about 0.1 for the 6 to 20-minute component of the fallout (and the associated $R_{i,95}$) values taken from the fractionation plots at $R_{89,95} = 0.1$) gives a reasonable agreement

between the isotopes analyzed for in common in both cloud and ground fallout samples. In Table 4.1 the results of the partition calculations are given for $\overline{R}_{89,95}$ (fallout) = 0.0317 and 0.0488. The latter value was composited from 75% of 0.032 and 25% of 0.10.

TABLE 4.1 PARTITION OF ISOTOPE ACTIVITY BETWEEN CLOUD AND FALLOUT

Isotope	Fallout Analysis		Cloud Analysis	
	$R_{89,95}=.0317$	$R_{89,95}=.0488$	$R_{89,95}=.0317$	$R_{89,95}=.0488$
^{89}Sr	0.023	0.035	0.977	0.965
^{90}Sr	0.08	0.13	0.94	0.93
^{91}Y	0.37	0.42	0.69	0.67
^{99}Mo	0.72	0.72	0.29	0.28
^{95}Zr	0.72	0.716	0.285	0.284
^{103}Ru	0.51	0.56	–	–
^{106}Ru	0.05	0.12	–	–
^{125}Sn	–	–	0.91	0.90
^{129m}Te	–	–	0.86	0.79
^{131}I	0.07	0.21	–	–
^{132}Te	0.05	0.14	0.88	0.82
^{137}Cs	0.05	0.08	0.98	1.00
^{140}Ba	0.20	0.27	0.80	0.72
^{141}Ce	0.42	0.34	0.61	0.60
^{143}Pr	–	–	0.29	0.28
^{144}Ce	0.76	0.75	0.29	0.28
^{147}Nd	–	–	0.26	0.25

The analysis yields reasonably consistent results. The data derived for $R_{89,95}= 0.0488$ probably describe the partition to a good approximation.

4.2.1 Partition of Debris Mass Between Cloud and Surface. The average specific activity based on Zr^{95} of the 20 to 30-minute minute cloud sample is 5×10^{13} fissions per gram. This cloud contains 29% of the Zr^{95} produced, or 0.142 kt. There are 1.4×10^{23} fissions/kt. It follows that the total mass debris in the cloud is 400 tons.

The mass of prompt fallout is at least $400 \times (0.715/0.185) =$ 1,000 tons. This follows because S_{95} in the cloud and in the intense prompt fallout is nearly identical. A higher total number than 1,000 tons for all fallout is indicated because throwout away from the hot-line has a lower average specific activity than the hot-line weighted average calculated in Table 3.10. The correct value for the total mass of prompt fallout is $(1000/\bar{S}) \ 5 \times 10^{13}$, where $\bar{S}$ is the truly weighted average S_{95} over the entire fallout grid.

4.3 SPECIFIC ACTIVITY AND MASS DISTRIBUTION MODEL

The data in Tables 3.6 and 3.9 provide the basis for testing a specific activity model in which activity is related to some power of the diameter. Thus, if $F(D)$ is the particle size distribution at a given altitude, then $D^n.F(D)$ will represent the activity distributions as a function of particle size if n is properly chosen for each isotopic species. The mass distribution should be described by $n = 3.0$. If further, n can be related to the slopes of the fractionation plots as tabulated in Figure 3.2, a quite general description of the system can be achieved.

4.3.1 Size and Activity Distribution Calculations in Benzene Fractions. In the benzene experiment, 0.8 of the 32.5 cm column was withdrawn for examination after each of six settling times. The residue from the 1-minute settling fraction was

64

filtered directly. A Stokes law sedimentation rate was
assumed, using particle and benzene densities of 2.50 and
0.88 gm/cm^3, respectively. The viscocity of benzene was
6.5 x 10^{-3} poise. The rate of fall of irregularly shaped
particles was taken to be 0.65 that of equivalent spheres.
For these conditions, the fall rate for a 1-micron diameter
particle is 8.7 x 10^{-5} cm/sec.

If f_i is the fraction of the original number of particles
of size D available at the beginning of each sequential
sedimentation, a function $\phi_i(D)$ is defined for each of the six
sedimentations, of the form:

$$\phi_i(D) = f_i \frac{(.8 \times 32.5 - 8.7 \times 10^{-5}D^2 t)}{32.5} \tag{4.1}$$

where D is the statistical diameter of the irregular particle,
in microns, and t is the settling time in seconds. The $\phi_i(D)$
functions obtained by this analysis are plotted in Figure 3.2.

Experimentally, the particle size distribution F(D) was
established to be of the form $K/D^{n'}$ from 1 to 60 microns. The
distribution functions in D^n are, therefore,

$$F(D^n) = D^n.F(D) = F(D^{n-n'}) \tag{4.2}$$

'n' has a preferred value of 3.25. Since in Table 3.6 the Cs^{137} and Ru^{106} always exhibit their maximum percentages in the 60-minute fraction rather than the 120-minute fraction, we explored the possibility that the active particle size distribution might have a maximum in the vicinity of 1 micron and fall off at lower values. Accordingly, a number median diameter D_g of 0.5, 1, 2, and 3 microns was employed, with symmetrical size distribution functions of the form:

$$K_1 D^{3.25} \; (0 \text{ to } D_g) \text{ and } K_2 D^{-3.25} \; (D_g \text{ to cut-off}) \tag{4.3}$$

The ratio K_1/K_2 required to normalize the number distribution was calculated for each value of D_g by setting

$$K_1/K_2 \int_0^{D_g} D^{3.2} \, dD = \int_{D_g}^{\infty} D^{-3.2} \, dD \tag{4.4}$$

The distribution functions for various values of n are:

$$F(D^n) = \frac{K_1/K_2 \int_0^{D_g} \phi_1(D) \cdot D^{3.25+n} \, dD + \int_{D_g}^{D} \phi_1(D) \cdot D^{n-3.25} \, dD}{K_1/K_2 \int_0^{D_g} D^{3.25} \, dD + \int_{D_g}^{D} D^{n-3.25} \, dD} \tag{4.5}$$

In Equation 4.5 the integration limit D_g is the assumed maximum in the size distribution, D is the cut-off value in

the cloud at the time and altitude of sampling. The adoption of D_g between 0.5 and 3 microns places 1 to 12 percent of the activity below D_g. The calculations were also performed with a lower integration limit of zero (no maximum).

The results of these calculations are tabulated in Appendix C. Mention will be made here of the differences between two independent settling experiments conducted with the 11K and 14K debris. The data in Table 3.6 were obtained using analytical grade benzene. Those in Table 3.9 were obtained in a later experiment with a lower grade benzene. Separations were less clean, as was evidenced by adherence of particles to the vessel wall. Unfortunately, weight percents corresponding to the activity percents reported in Table 3.6 were not recorded. In the succeeding discussion data for the second experiment will be also used, since the mass percentages in each fraction are available. However, we believe that Table 3.6 represents a better description of nuclide activity in the first five, and in the sixth and seventh particle size fractions and the comparisons with the calculations in Appendix C will be used as a basis for choosing the best values of n to describe the distribution of activity with size of Zr^{95}, Ce^{144}, Ru^{106}, and Cs^{137}. (The separations achieved between the one-minute settling and the residue fraction were highly variable and technique dependent).

67

Calculated and observed mass and isotopic distributions

for the 11K and 14K debris, as found in the second experiment,

are given in Table 4.2. The data are best fit using a $D_{cut-off} =$

100 microns for 11K and 76 microns at 14K. There is little

difference resulting from the choice of a lower limit of integra-

tion of zero, with no maximum, or $D_g = 0.5$ micron.

The data of Table 3.6 give a different picture for the Cs^{137}

and Ru^{106} distributions, with values of n being ~.2 unit lower.

In Table 4.3, the choice of n was largely dictated by

the fit observed in the combined and 1-minute fractions. D_g was

taken as 0.5 micron. The cut-offs assumed at 9.5K, 11K, 13.5K,

and 14K were, respectively, 137, 120, 76, and 76 microns,

respectively. These values differ somewhat from those given

in Table 3.5. The proper choice of the cut-off value in the

13.5 sample is particularly ambiguous, since sampling was

conducted at 12K and at 13.5 through 14K. (In Table 4.2 a value of

100 microns for the 11K samples was shown to give the best

fit.) In Table 4.3 the comparison between calculated and

observed values for Zr^{95} are applicable as well to Ce^{144}.

The following conclusions can be drawn:

(1) The agreement is not good for fitting the percentages

of Cs^{137} and Ru^{106} in the 120-minute, 60-minute, and 30-minute

fractions for any choice of D_g, $D_{cut-off}$ or n. Too much

activity is always placed in the 120-minute fraction. The best fits for the distributions of Cs^{137} and Ru^{106} in the courser fractions (5 minute, 1 minute, and residue, with cut-offs greater than 18 microns) is given for n = 1.9 - 2.2 for Cs^{137} and 2.2 - 2.4 for Ru^{106}. These choices of n give the observed partition of Cs^{137} and Ru^{106} between particles less than 18 and greater than 18 microns, to good approximation. A reasonable explanation for the distribution of these isotopes in the smaller size fractions may be that Cs^{137} (and to a lesser degree Ru^{106}) distribute themselves with variable n over the particle size range and that the maximum in the active particle frequency function is indeed shifted to values in excess of 5 microns. Further analysis will be required to clarify this point. Many of the inconsistencies noted in comparing Tables 4.2 and 4.3 are unquestionably due to limitations in reproducing clean-cut separations experimentally. Another ambiguity arises from the proper choice of cut-off diameters at the sampling altitudes in question. However, for purposes of deducing values of n appropriate to partitioning the cloud debris between nuclide activity in fractions less than and greater than 18 microns, and for deriving a relationship between the slopes of the cloud fractionation plots and n, it suffices to use n values which fit the courser fractions. Thus, n = 2.00 will fit Cs^{137} and n = 2.25 Ru^{106}.

69

(2) A fair fit can be achieved for the mass distribution with n=3. This confirms the choice of $F(D) = K/D^{3.25}$ as a good description of the particle size distribution at all altitudes out to the cut-off values.

(3) The distribution of Zr^{95} and Ce^{144} is rather well accommodated by n = 2.8+.1 in all courser fractions. (The 1-minute fractions at 9.5K and 14K in Table 4.3 are notable exceptions). The agreement is fair even in the smaller size fractions, although again the 120-minute fraction as calculated is usually too high.

4.3.2 The n Parameter and the Slope of Fractionation Plots. The n parameter varies between 2.0 and 2.8 for the isotopes exhibiting extreme fractionation behavior, Cs^{137} and Zr^{95}. The slopes of the fractionation plots of Figure 3.1 vary from -0.04 to 1.0, or 0.8n units per 1.04 slope units. In Table 4.4 are listed the slopes and corresponding interpolated n values.

4.4 PARTITION BETWEEN INTERMEDIATE AND DISTANT FALLOUT

Sufficient facts are at hand to establish the ultimate fate of the radioactive and inert components of the 20-minute

cloud, given the meteorological conditions. These facts are:

(1) The total mass of airborne debris, its particle size distribution, and its variation with altitude.

(2) The cloud inventory of 17 fission product radio-isotopes and the variation in radiochemical composition and concentration with altitude.

(3) The relationship between particle size and radio-chemical composition as given by the n values in Table 4.4.

This problem will not be treated comprehensively. Only the salient points will be indicated.

4.4.1 Cloud Fallout of Debris and Radioactive Isotopes in Greater than 18 Micron Fraction. Material residing in particles larger than 18 microns diameter will have fallen to sea level in from 52 to 76 hours. This component of the cloud, which may be termed intermediate, will now be estimated.

The specific activity of the refractory isotopes Mo^{99}, Zr^{95}, Ce^{144}, and other rare earths are reasonably constant in the cloud debris as a function of altitude. $S_{95} = 4.1 \times 10^{13}$ F/gm at 11K and 5.5×10^{13} F/gm at 14K. Thus, both the debris and isotopes can be treated together in good approximation. Accordingly we will assume a particle size distribution for the whole cloud of the form $K/D^{3.25}$ with a cut-off at 100 microns.

71

This cut-off value is intermediate between the values obtaining for the top and bottom of the cloud. In any event, the results are relatively insensitive to the cut-off diameter adopted, as the calculations in Appendix C illustrate.

Thus, the fraction of isotope or mass falling out associated with particles greater than 18 microns is:

$$\phi_n \qquad \frac{\int_{18}^{100} D^{n-3.25}\, dD}{\int_{0}^{100} D^{n-3.25}\, dD} \qquad\qquad (4.6)$$

where n is the value listed in Table 4.4.

In Table 4.5, Column 1 is the percent of cloud isotopic activities associated with particle sizes greater than 18 microns obtained from Equation 4.6. Column 2 is the percent of the total isotope made by the device residing in cloud particles greater than 18 microns. Column 3 is the percent of the total isotope made by the device residing in cloud particles less than 18 microns. It represents the material available for long range fallout, capable of being transported to great distances.

The calculated mass in cloud particles greater than 18 microns is 73.5%. Hence the absolute mass in this size range is 400 x 0.735 = 294 tons. The choice of a lower cut-off diameter would tend to raise somewhat the figures in the final column.

For comparison we give the observed percentages of total activities in the 5m, 1m, and residue fractions, corresponding roughly to >18 micron particles, taken from Table 3.9.

	9.5K	11K	12-14K	14K
Cs^{137}	21.2	31.7	35.3	14.0
Ru^{106}	35.5	49.5	41.2	23.5
Zr^{95}	69.8	73.6	66.1	55.0
Ce^{144}	71.7	73.0	68.3	52.8

If these values are weighted by the intensity profile given in Table 3.1 to represent the average composition in the cloud, the results are in fair agreement with Column 1, Table 4.5.

Cs^{137}	24.1
Ru^{106}	33.8
Zr^{95}	62.6
Ce^{144}	62.2

4.5 PARTICLE SIZE AND MASS FREQUENCY CURVES FOR THE EVENT

The salient features of the particle size and mass frequency curves for the event can be deduced from a synthesis of NRDL and our data. A crude normalization might be provided by using the fact that there are approximately 400 tons of debris in the 20-minute cloud and of the order of 1,000 tons of high specific activity prompt fallout.

The particle size distribution found in the 20-minute cloud appears to be given by $K/D^{+3.25}$ to good approximation between 1 micron and the cloud cut-offs (100 to 160 microns). This implies a mass distribution as $D^{-0.25}$ in the cloud. The NRDL data (see summary in Table 3.11) exhibit a median mass diameter of 700 to 1,000 microns in the more intense fallout (it is lower elsewhere) and a median activity diameter (MAD) ꜜꜜꜜꜜꜜꜜꜜꜜꜜ ꜜꜜꜜꜜꜜꜜ ꜜꜜꜜꜜ ꜜꜜꜜ ꜜꜜꜜ. Clark, in Reference 8 has observed that the fraction of radioactive particles increases with size in the fallout, being about 25 to 50 percent in the larger size fractions (>200μ). This finding is in accord with our observation that the mean specific activity of the prompt fallout $S_{95} = 5.7 \times 10^{13}$, whereas the specific activity of the lava particles, which represent the main active component, is 1.88×10^{14} or approximately three times higher. Further, the specific activity of lava particles is reasonably constant.

The question of selecting a particle-size distribution for the event has not been studied in detail, but it is evident that the active mass distribution, over the entire particle size range in the fallout samples, is relatively flat, i.e., $dM/dD \sim$ constant to within a factor of 5, and the particle size distribution is therefore crudely of the form k/D^3. While these conclusions are of qualitative worth at best and although Johnie Boy is probably an atypical case, they suggest the inadequacy of a monomodal, log-normal particle size distribution peaking at 120 microns, such as is used in some current fallout models. The rather good agreement between the predicted and observed fallout patterns, as reported in Reference 9, is somewhat fortuitous, since the particle-size distribution used in the model bears little relationship to that which actually characterized the event.

4.6 SPECIFIC ACTIVITY AND ENERGY COUPLING

In a situation wherein the energy of the device is effectively coupled with the soil environment, the specific activities of refractory isotopes should be fairly uniform in both cloud and fallout debris. This is the case in Johnie Boy. However, the average S_{95} of about 5×10^{13} F/gm found both in cloud and intense fallout samples is only about 15% of the value expected if fission zirconium were uniformly

75

incorporated in volatilized and recondensed soil. The lava-like particles found on the hot-line, and exhibiting S_{95} values of 2×10^{13} F/gm on the average, with one as high as 2.8×10^{14}, meet the criterion of efficient incorporation. This suggests that the agreement between cloud and fallout S_{95} may be an irrelevant fortuity. Both phases were diluted about seven-fold with inert material. (Dilution factors off the hot-line were, of course, much greater). In fact, S_{95} values in the cloud samples are a factor of two higher in the small than the large particles (see Table 3.9). The drop-off of S_{95} in the smallest particle size fraction in the cloud is attributed to the high preshot atmospheric dust content blank.

As energy coupling with the environment decreases, the fraction of fused and volatilized soil mass decreases. However, considerable masses of inert materials may still be moved. (Compare Jangle S with Jangle U). While the average specific activity for the event must be higher than for the more efficiently coupled case, and the average specific activity for the persistent cloud debris must certainly be higher, the prompt and long-term fallout may exhibit a wide spectrum of values, above and below 3×10^{14} F_{95}/gm. This interesting point, relating to the scaling of surface burst

phenomenology, calls for a reexamination of past data. A
first step is to examine the relationships between moved
mass and volatilized mass as they relate to yield and to
condition of burst.

The specific activity of volatile isotope chains (Sr^{89},
Cs^{137}, Ba^{140}, Sr^{90}, Y^{91}, Ce^{141}, I^{131}, Te^{132}) in the fallout
and cloud samples is obviously related to yield as well as
to energy coupling in any incompletely contained situation.
In the Johnie Boy case coupling was very effective in physically
separating the volatile and refractory chains between fallout
and cloud. The buoyant bubble cooled rapidly (some energy
had been dissipated in soil volatilization), prior to the
growth of chain members of more refractory character. Hence
a physical separation of the main mass of the debris was
achieved from the vapor constituents still rich in the halogens,
rare gases, and alkali metals. At higher yields and longer
condensation times, greater fractions of the aforementioned
chains will be incorporated into the larger particles, along
with Zr^{95} and Ce^{144} because more of the chains will exist
as the alkali and alkaline earth metals, at the time the debris
is forming (before it leaves the cloud). This will lead to
a less pronounced partition of volatile chain isotopes between
persistent cloud and fallout.

77

4.7 FRACTIONATION AND PARTITION BETWEEN PROMPT AND LONG RANGE
FALLOUT

The relationship between fallout partition and fractionation will now be examined. The partition equation, using Zr^{95} as the refractory and Sr^{89} as the volatile prototypes is:

$$\frac{F_{95}(\text{fallout})}{F_{95}(\text{cloud})} = \frac{R_{89,95}(\text{cloud}) - 1}{1 - R_{89,95}(\text{fallout})}$$

(4.7)

This expression is obviously indeterminate when $R_{89,95}(\text{cloud}) = R_{89,95}(\text{fallout})$, and it becomes less useful as they approach each other. A further constraint is that the $R_{89,95}$ values be properly weighted averages.

In Johnie Boy the situation was ideal for application of Equation 4.7. A more interesting use of this tool is to reexamine cloud and fallout radiochemical data from high-yield surface bursts with a view to finding a relationship between partitioning of the isotopes and total yield. For those cases in which the data are incomplete, but cloud and fallout samples are still on hand, the techniques used in this report can be used to establish the relationship between particle size and the isotopic content of Cs^{137}, Sr^{90}, and Pm^{147} in the cloud samples. These three isotopes

SECRET

are typical of volatile, intermediate, and refractory chains. All have half lives suitably long for this purpose, even twelve years after the fact.

An important source of relevant information should not be overlooked. Stratospheric and tropospheric sampling and analysis programs, such as HASP, especially when conducted during nuclear testing, can yield information on the isotopic composition of the persistent atmospheric reservoir. If the R values of Cs^{137}, Sr^{90}, and Ce^{144} attributable to specific events, or groups of events, are close to their thermonuclear production ratios, which are well established, and the fallout samples exhibit a significant alteration from normal values, a rather precise statement of the partition is had.

Implicit in any physical reasoning attached to the use of Equation 4.7 is that radiochemical composition is related to particle size. If Cs^{137} and Zr^{95} were uniformly distributed in large and small particles alike, there would be no fractionation and the equation cannot be used. A critical examination of thermonuclear fallout data from this point of view is indicated. As suggested in Section 4.6, higher yields give longer condensation times and therefore more uniform radiochemical composition.

4.8 SIGNIFICANCE OF LOGARITHMIC FRACTIONATION CORRELATIONS

In Section 4.4 use was made of the slopes of the fraction-
ation plots of the cloud samples to establish a relationship
between particle size and isotopic composition. This procedure
was justified on the demonstrated relationship between particle
size and isotopic composition in the 28 laboratory fractionated
samples.

In Section 4.1 the isotopic composition of the prompt
fallout samples was shown to be related in a semi-quantitative
fashion to a time of particle formation . The calculation
introduced no geometric concepts of area or volume, and, in
fact, was found to apply to a group of fallout samples in which
no pronounced relationship between particle size and radio-
chemical constitution exists (see Reference 9).

Further, the cloud and fallout sample data do not form
a continuous set on a fractionation plot. If the cloud data
are extrapolated to $R_{95,89}$ values characteristic of the fallout
samples, using the slopes observed in the cloud samples,
the fallout composition is not obtained. The inverse
is obviously true for the fallout samples. A plausible basis
for this result is to be found in Figure 4.1. $R_{i,95}$ values,
as calculated, are seen to approach a value of 1.00 asymptotically
as Sr^{89}/Zr^{95} approaches 1. If a straight line extrapolation

SECRET

of the Sr^{90}/Zr^{95} data were made by drawing a line through the experimental points with a slope of about 1.05, the Sr^{90}/Zr^{95} in the cloud sample would be over-estimated by a factor of 4.4. While, in the absence of other information, a straight line can be drawn through the datum points of Figure 4.1 and fit the data better than the theoretical curve with constantly changing slope, the latter corresponds to a more physically comprehensible picture and does not lead to unreasonable values for the extrapolated composition of the cloud samples. It does, however, leave unanswered the basis for the cloud fractionation plots (Figure 3.1).

It should be pointed out that there is an element of arbitrariness in the way the lines are drawn in Figure 3.1. With the exception of the Nd^{147} line, which is drawn parallel to the Mo^{99} line, the lines were drawn to converge at 1.0. This is physically reasonable and certainly within the allowed error in the individual datum points, estimated to be about 10%. (Our Nd^{147} relative counting efficiency is probably 10% too high.) This arbitrariness does not affect the argument advanced in the preceeding paragraph.

The slopes of the cloud fractionation plots are evidently directly related to the partition of the individual radio-isotopes between cloud and fallout. In fact, the ordinate

81

at $R_{95,89} = 0.29$ is the fraction of the device activity of tne particular isotope in question which is found in the cloud, to within a few percent.

We note that by definition, the range of slopes is from 1 to 0 if the abscissa is chosen as the R value of the most refractory with respect to the most volatile isotope, and the ordinate is taken with respect to the volatile archetype. If an isotope is as volatile as Cs^{137} it will have a zero slope; if as refractory as Zr^{95} a unit slope. This fact provides a convenient basis for assigning to each isotope a power $(2 + n)$, where n is related to the slope of the fractionation plot, to describe the relationship between the particle size and specific activity.

It is evident that a log-normal distribution is not required to yield a straight line on a logarithmic plot when activity is incorporated into the particle in accordance with some power of the diameter. In the Johnie Boy samples tne power law fit $D^{-3.25}$ leads to the same result.

The slopes given in Reference 1 for coral island surface shots are compared in Table 4.6. Recalling that the coral surface slopes of the logarithmic fractionation correlations pertain to high-yield bursts, the higher values of the slopes for Sr^{90}, Te^{132}, and Ba^{140}

are quite reasonable. Condensation times are much longer than for Johnie Boy. In the instances of chains 90 and 140, a greater fraction can decay to alkali and alkaline-earth elements while the cloud is still hot and well mixed, thus permitting a more uniform incorporation with Zr^{95} and the refractory isotopes. The distinctly different behavior of U^{238} (reported by Freiling as Np^{239}) is most interesting and may be related to differences in particle matrix character.

To explain the relationship in the cloud samples between specific activity and particle size, the surface-to-volume concept of Freiling has much merit. A comparison of the calculated percentage of activity of Zr^{95} and Ce^{144} between the twenty eight benzene fractions with those recorded in Table 3.6 reveals that the activity distribution of Zr^{95} is best fit by a $D^{2.8 \pm .1}$ relationship. However, a choice of $D^{3.0}$ would place too much of the refractory isotopes in the larger sized fractions (>18 microns). The close similitude to volumetric incorporation of Zr^{95} in the cloud samples may be interpreted to argue in favor of the assumption that Zr^{95} is reasonably uniformly distributed throughout the radioactive particles. However, two physical factors may be at work to artefact this behavior. The low specific activity of Zr^{95} (1/5th to 1/7th that expected for volatilization of the

matrix and zirconium incorporation in the condensate) suggests a primarily surface adherence and subsequent agglomeration of heated, finer soil particles. Further, the surface-to-weight ratio for highly irregular particles over the particle size range in question may lead approximately to the calculated volume-to-weight ratio of equivalent spheres. From a pragmatic point of view it suffices to treat the Zr^{95} and its refractory analogues in this event as exhibiting close to a D^3 relationship in specific activity and to treat Cs^{137}, the most volatile isotope, as being incorporated as D^2, bearing in mind the inconsistencies produced in the particle fractions <18 microns.

It is tempting to interpret the slopes of the fractionation plots in terms of the partition of the isotopes between cloud and fallout for the general case. However, as a corollary to the discussion in Section 4.7, two facts are still needed: the percent of the reference isotope (Zr^{95} or Sr^{89}) in the cloud and the average value of $R_{i,89}$ or $R_{i,95}$ in the cloud.

TABLE 4.2 CALCULATED AND OBSERVED ISOTOPIC DISTRIBUTIONS

Fraction	%M	$D^{3.0}$	%Zr^{95}	$D^{2.8}$	%Cs^{137}	$D^{2.3}$	%Ru^{106}	$D^{2.4}$
				11K				
120m	5.20	8.33	10.3	11.1	19.5	45.2	17.0	37.2
60m	4.55	4.58	8.7	5.6	17.8	13.8	16.9	12.6
30m	6.20	4.21	8.8	4.6	16.9	6.6	15.5	6.7
15m	5.44	4.96	5.8	5.4	10.9	5.1	9.9	5.7
5m	7.31	9.32	6.0	9.6	8.8	6.4	8.0	7.5
1m	25.3	21.8	20.0	20.9	13.0	9.5	13.9	12.6
residue	44.4	46.8	40.4	42.1	13.0	13.0	18.8	17.0
				14K				
120m	3.34	9.0	3.1	15.2	4.0	43.5	8.5	36.8
60m	10.3	5.2	17.0	7.5	22.0	14.0	22.6	12.8
30m	8.3	5.0	13.3	6.1	17.1	7.0	18.9	7.2
15m	11.0	6.0	14.6	6.5	18.4	5.6	18.9	6.2
5m	10.9	11.8	10.2	11.6	12.4	7.4	19.8	8.6
1m	23.2	28.0	16.4	24.8	15.2	11.2	17.0	14.1
residue	33.1	34.0	25.4	28.0	10.9	11.0	13.2	14.1

SECRET

TABLE 4.3   CALCULATED AND OBSERVED ISOTOPIC DISTRIBUTIONS
(First .Benzene Experiment)

9.5K

Fraction	$\%Zr^{95}$	$D^{2.75}$	$\%Cs^{137}$	$D^{2.00}$	$\%Ru^{106}$	$D^{2.25}$
120m	5.5	10.3	18.6	45.9	12.3	32.1
60m	11.6	5.5	31.1·	15.5	26.4	12.4
30m	8.2	4.6	19.7	7.6	15.5	7.4
15m	4.9	5.0	9.7	5.4	10.3	6.2
5m	3.9	8.6	5.2	6.2	5.5	8.1
1m	4.5	17.5	4.6	7.8	8.8	12.0
residue	61.4	48.5	11.4	11.6	21.2	21.8

11K

Fraction	$\%Zr^{95}$	$D^{2.75}$	$\%Cs^{137}$	$D^{2.00}$	$\%Ru^{106}$	$D^{2.25}$
120m	4.0	11.1	11.3	46.4	8.1	32.8
60m	8.7	5.9	22.3	15.6	17.8	12.7
30m	6.7	5.0	17.9	7.7	13.5	7.5
15m	7.5	5,4	16.6	5.5	11.2	6.3
5m	6.1	9.2	10.2	6.2	12.4	8.3
1m	10.8	18.8	9.7	7.9	12.7	12.3
residue	56.7	44.8	11.8	10.7	24.4	20.1

12-14K

Fraction	$\%Zr^{95}$	$D^{2.75}$	$\%Cs^{137}$	$D^{2.25}$	$\%Ru^{106}$	$D^{2.35}$
120m	6.7	14.1	14.2	35.6	13.4	29.6
60m	12.0	7.5	22.5	13.8	20.0	12.2
30m	7.7	6.3	15.1	8.2	10.6	7.9
15m	7.7	6.9	12.9	6.9	14.8	7.1
5m	7.4	11.7	9.6	9.0	7.5	10.0
1m	24.9	24.0	14.4	13.3	18.4	16.1
residue	33.9	29.6	11.3	13.2	15.3	17.1

14K

Fraction	$\%Zr^{95}$	$D^{2.75}$	$\%Cs^{137}$	$D^{1.88}$	$\%Ru^{106}$	$D^{2.25}$
120m	4.4	14.1	10.3	53.5	8.2	35.6
60m	17.0	7.5	34.6	16.9	26.4	13.8
30m	17.0	6.3	30.5	7.0	32.5	8.2
15m	6.6	6.9	10.7	5.0	9.3	6.9
5m	6.8	11.7	4.8	5.3	5.1	9.0
1m	5.6	23.9	3.6	6.3	4.6	13.3
residue	42.6	29.6	5.6	5.4	13.8	13.2

TABLE 4.4   FRACTIONATION SLOPES AND n PARAMETER

	Slope	n
Cs^{137}	-0.04	2.00
Sr^{89}	0.00	2.03
Sr^{90}	0.02	2.06
Sn^{125}	0.07	2.09
$Te^{132}(I^{131})$	0.12	2.13
Te^{129m}	0.16	2.15
Ba^{140}	0.20	2.19
Ru^{106}	0.20	2.19
Y^{91}	0.28	2.25
Ce^{141}	0.38	2.32
Ru^{103}	(0.50)	2.41
Mo^{99}	1.00	2.80
Zr^{95}	1.00	2.80
Pr^{143}	1.00	2.80
Ce^{144}	1.00	2.80
Nd^{147}	1.00	2.80

The values for I^{131} and for Ru^{103} in the above table are assumed on the basis of their behavior in the fallout debris. The interpolated n values should give to a fair degree the distribution of debris between 0 and 18 microns and from 18 microns to the cut-off diameter.

SECRET

TABLE 4.5   ISOTOPIC PARTITION BETWEEN LONG RANGE AND
            INTERMEDIATE FALLOUT

Isotope	% Cloud Activity >18μ in cloud	%Total Activity >18μ in cloud	%Total Activity <18μ in cloud
Cs^{137}	23	22	78
Sr^{89}	24	24	74
Sr^{90}	26	24	69
Sn^{125}	27	25	65
Te^{132}	29	26	56
(I^{131})	29	26	53
Te^{129m}	30	26	53
Ba^{140}	32	26	54
(Ru^{106})	32	26	42
Y^{91}	35	24	43
Ce^{141}	39	24	36
(Ru^{103})	44	22	22
Mo^{99}	66	19	9
Zr^{95}	66	19	9
Pr^{143}	66	19	9
Ce^{143}	66	19	9
Nd^{147}	66	19	9
Mass	74	-	-

TABLE 4.6   COMPARISON OF CORAL SURFACE AND CONTINENTAL SURFACE
            SLOPES

	Coral Surface	Johnie Boy
Sr^{90}	0.24	0.02
Mo^{99}	1.10	1.00
Te^{132}	0.40	0.12
Cs^{137}	-0.03	-0.04
Ba^{140}	0.37	0.20
Ce^{144}	0.92	1.00
U^{238}	1.02	.22
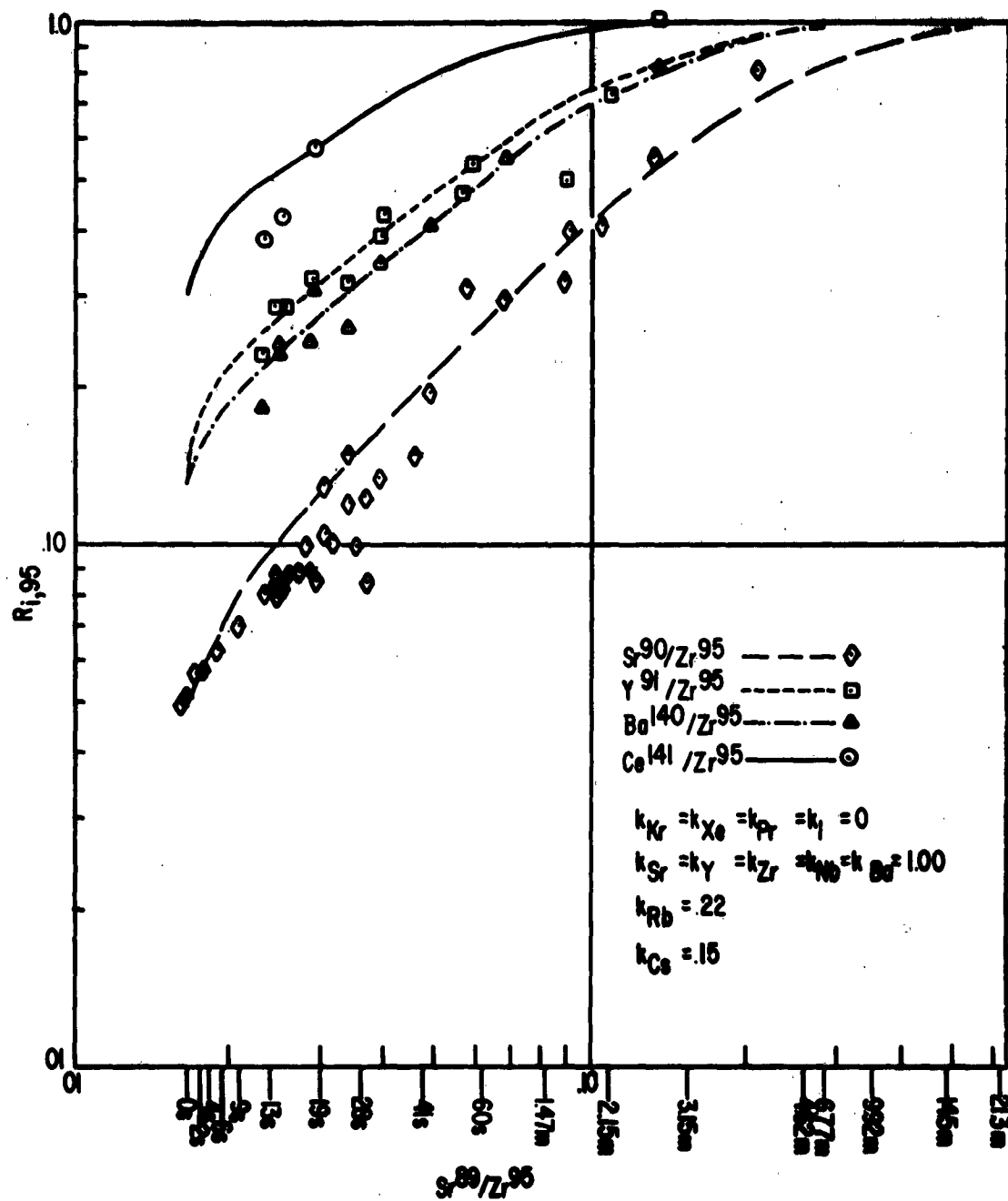
Figure 4.1 Fallout formation time and $R_{1,95}$.

SECRET

CHAPTER 5

CONCLUSIONS AND RECOMMENDATIONS

5.1 CONCLUSIONS

(1) The partition of Johnie Boy debris between prompt and delayed fallout has been established for 17 radioisotopes. Subsequent analysis can treat other fission product chains on an analogical basis.

(2) The radiochemical composition of prompt fallout debris has been described semi-quantitatively for five fission product chains using the concept of fallout formation time and physically reasonable attachment coefficients for the elements. A more rigorous and comprehensive model can probably be developed describing the fractionated composition of all isotopes in prompt fallout.

(3) The specific activity as a function of particle size has been semi-quantitatively formulated for four radio-isotopes. Specific activity-particle size relationships for cloud debris samples can probably be generalized on the basis of the slopes of logarithmic correlation plots of cloud debris samples.

(4) The particle size distributions of the prompt fallout and of the cloud are not in agreement with current particle size models.

(5) The slopes of logarithmic correlation fractiona-
tion plots are related to but are not unique indices of
isotope partition between cloud and prompt fallout. Straight
lines fitting cloud fractionation data are not extrapolable
to the composition of fallout samples.

(6) The comprehensive description of a fallout event,
to include radioisotope partitioning between cloud and prompt
fallout, in order to yield insights on the basis of which yield
scaling laws can be developed, requires as a sine qua non exhaustive
radiochemical and physical definition of both radioactive
cloud and the prompt fallout.

5.2 RECOMMENDATIONS

(1) This study is not yet completed. A number of aspects
of the problem have been treated with less than the desired
rigor and should be pursued further either by this or other
laboratories. Among these are: the active versus the non-
active particle size distributions in the cloud debris; a better
analytical description of the distribution of Cs^{137} activity in
the various benzene fractions; a better choice of the average
Sr^{89}/Zr^{95} ratio characteristic of the prompt fallout, taking
into account the fallout between 6 minutes and 20 minutes,
a factor largely glassed over in the preceeding analysis;

91

a better definition of the particle size distribution of the active particles in the prompt fallout; a more complete and satisfying treatment of predicting the composition of prompt fallout particles, particularly with respect to the iodine isotopes.

(2) If future opportunities are provided for studying fallout situations, equal emphasis should be given ground and aerial sampling and analysis programs.

(3) The methods used in this study, or more unhurried and sophisticated versions thereof, can be applied profitably to the post-facto investigation of selected ground burst events over a range of yields, where aerial samples still exist. The knowledge gained of the particle size distribution of cloud samples, and the relationship between particle size and radiochemical composition for Sr^{90}, Cs^{137}, and Pm^{147}, can be invoked after the fact, in conjunction with analyses already a matter of record, to assist in the partitioning of the debris between prompt, intermediate, and long range fallout, as a function of yield and burst condition.

SECRET

Appendix A

CLOUD PENETRATION

PROCEDURE

Cloud penetration samples were collected by three B-57 sampling aircraft for this project. The aircraft penetrated the Johnie Boy cloud at different altitudes and times after detonation (Table A.1).

Although some modifications of the procedures were made during the experiment just prior to the penetrations, the general procedure for the collection of samples by the aircraft were the same. An aircraft was to penetrate the cloud at a designated altitude and time after detonation in straight and level flight and collect a sample in one of the wing tip sample collectors. After emerging from the cloud, the aircraft would again penetrate at another altitude and collect a sample with the other wing tip sample collector.

The crew was furnished a data card for recording time of entry and exit of the cloud, maximum dose rate recorded in the cloud, total dose during penetration, airspeed, altitude, temperature, and general comments on the size and shape of the cloud.

Immediately after a cloud penetration, the aircraft landed and the crew members were removed from the aircraft and monitored by a Rad Safe team. The aircraft was monitored and the wing tip samples were then removed and placed in individual lead pigs.

93

DISCUSSION

The Johnie Boy event was detonated one foot below ground at the Nevada Test Site on 11 Jul 62 at 0945 hours. The cloud reached a height of approximately 14,000 feet MSL and ground zero was 5,200 feet MSL.

Three B-57 aircraft from the 1211th Sampling Squadron at Kirtland Air Force Base, New Mexico, performed the cloud penetrations. Two of the aircraft were airborne prior to H-hour and penetrated the cloud from H+20 to H+33 minutes. The third aircraft was dispatched at H+20 minutes and penetrated the cloud at H+48 and H+54 minutes.

The data as recorded by the crew during the cloud penetrations are presented in Table A.2.

Photographs of the cloud at H + 25 seconds, H + 1 minute 30 seconds, and H + 2 minutes 30 seconds, are shown in Figures A.1 through A.3.

After the samples were removed from the aircraft wing tips, they were monitored and placed in lead pigs. The filter sample from a single wing tip tank is divided into a half and two quarter samples. Each of these sections was placed into a single lead pig.

The data obtained from the samples immediately after their removal from the aircraft appear in Table A.3. The data obtained on the samples at H+24 hours appear in Table A.4.

94

TABLE A.1 DOSE AND DOSE RATE DATA FROM CLOUD PENETRATIONS

MSL Altitude of Penetration (ft)	14,000	11,000	11,000	9,500	12,000	13,500 rising to 14,000
Penetration Time (min)	H+20	H+20	H+25	H+33	H+48	H+54
Peak Dose Rate in Cloud (r/hr)	200	60	60	6	0.1	8
Average Dose Rate in Cloud (r/hr)	75	10	30	4	0.05	4
Time Spent in Cloud (sec)	17	10	15	30	68	83
Total Dose (R)	0.6	0.2	0.3	0.45	0.01	0.35

TABLE A.2 DATA EXTRACTED FROM PILOTS DATA CARDS

Aircraft Number	827	842	842	842	245	245
Pass Number	1*	1**	2**	3***	1****	2****
Altitude (feet)	14,000	11,000	11,000	9500	12,000	13,000 rising to 14,000
Air Temp. (°C)	18	20	22	21	24	22
Time After H-Hour (minutes)	20	20	25	33	48	54
RASCEL Dose Rate Peak / Avg. In Cloud (r/hr)	200 / 75	60 / 10	60 / 30	6 / 4	0.1 / 0.5	8 / 4
Time in Cloud (sec.)	17	10	15	30	68	83
INTEGRON Dose (r)	0.6	0.2	0.3	0.45	0.01	0.35
RASCEL Cockpit Background (out of cloud) Dose Rate (r/hr)	0.4	0.05	0.1	0.1	0.01	0.15
Wing Tip Ion Chamber Dose Rate (r/hr)	1.2	0.05	0.05	0.2	0.23	0.47
IAS (knots)	250	250	250	250	250	250
Readings After Landing						
RASCEL (r/hr)	0.19	0.05	--	--	0.12	--
INTEGRON (r)	0.7	0.5	--	--	0.49	--
Ion Chamber (r/hr)	0.8	0.14	--	--	0.35	--
Time of Reading (min.)	H+33	H+50	--	--	H+75	--

*One penetration with both tip tanks open.

** Both passes made with left tank open, therefore, they represent one sample.

*** Only the right tip tank open.

**** Both penetrations made with both tanks open. The altitude variation of the second penetration was an attempt to follow the top of the cloud.

SECRET

TABLE A.3   DATA FROM SAMPLES IMMEDIATELY AFTER REMOVAL FROM AIRCRAFT

Aircraft Number	Paper Position*	Pig Gamma Reading at 7" - (r/hr)	Time of Reading	Missions Corrected to	Sample Size
827	L-1-1	1000	1057	4.2×10^{14}	Half
827	L-1-2	360	1059	1.5×10^{14}	Quarter
842	R-2	140	1111	7.5×10^{13}	Half
842	R-1-2	80	1115	4.5×10^{13}	Quarter
842	L-2	420	1119	1.9×10^{14}	Half
842	L-1-1	160	1121	1.1×10^{14}	Quarter
842	L-1-2	175	1122	1.2×10^{14}	Quarter
245	R-1-1	170	1158	1.9×10^{14}	Quarter

*Paper position R or L indicates right or left wing tip tank respectively.

TABLE A.4   DOSE RATE READINGS ON SAMPLES AT H + 24 HOURS

Position of Dose Rate Reading	245-R-1-1	842-R-2	842-L-1-1	842-L-1-2	842-R-1-2	827-L-1-1	827-L-1-2	842-L-2
At the surface of the pig with the pig closed.	5	10	25	12	3	30	25	40
At the mouth of the pig with the pig open.	100	--	90	60	12	250	130	190
On the surface of a 1-inch-diameter plastic vial containing a 1-square-inch piece of the sample.	9	2.3	6	4	0.6	16	7	7

Figure A.1 Aerial view of Johnie Boy event at H + 0 minutes, 25 seconds. (PCWT DASA 719-8-NTS-62)

98

Figure A.2   View of Johnie Boy event, H + 1 minute, 30 seconds.
(FCWT DASA 719-7-NTS-62)

99

Figure A.3   Aerial view of Johnie Boy event, H + 2 minutes, 30 seconds.
(FCWT DASA 719-10-NTS-62)

100

SECRET

Appendix B

PARTICLE SIZE AND SPECIFIC ACTIVITY MEASUREMENTS

Introduction

The early penetration air samples from the Johnie Boy test were used to determine the distribution of the various radioactive nuclides with respect to particle size. Included were fission product analysis of the samples at various altitudes, particle size separation by settling methods, classification of the particle sizes by microscopy techniques, and gamma spectroscopy of the various size particles from each of the attitudes.

The particle size separation was accomplished by dry ashing the filter papers, stirring the remaining particles in a graduated cylinder containing benzene, and separating and filtering the top four-fifths of the liquid after settling times of 120, 60, 30, 15, 5, and 1 minute respectively. These samples were split into two portions, 1/4 being used for particle sizing and 3/4 being reserved for gamma spectrometer analysis.

Aerial Sample Usage

Following is a listing of the manner in which the aerial samples were used.

101

Aircraft Number	827	827	842	842	842	842	842	245
Task Number	L-1-1	L-1-2	R-2	R-1-2	L-2	L-1-1	L-1-2	R-1-1
Altitude(s) (1,000 ft)	14	14	9.5	9.5	11	11	11	12-14
Time(s) of Penetration (Min)	20	20	33	33	25 20	25 20	25 20	48 54
Amount of Paper Received	1/2	1/4	1/2	1/4	1/2	1/4	1/4	1/4
Fission Product Analysis	-	1/4	1/2	-	-	1/4	-	1/8
Particle Sizing	1/8	-	-	1/8	3/16	-	-	1/16
Particle Reserve	1/16	-	-	-	1/16	-	1/8	-
Mixed Fission Product Source	5/16	-	-	1/8	1/4	-	1/8	1/16

Sample Preparation for Particle Sizing

The samples of IPC paper were placed in beakers and ashed in a muffle furnace at 450°C for approximately 16 hours; some of the samples were ashed up to 8 hours longer because of remaining carbonaceous material.

The amount of residue for blank IPC paper was found to be only 11.1 mg per square foot of paper. A full aerial IPC paper would have an area of 4.75 square feet and has 52.7 mg of residue.

By using this blank the following calculations were made to determine the weight of particles that were on the filter paper. The diameter of the filter paper is 30 inches and the diameter of the sampling area is 29 1/2 inches.

Aircraft Number	827	842	842
Tank Number	L-1-1	L-1-2	L-2
Radius of Sampling Area (r_s)	14"	13"	14"
Length of Arc of Sampling Area (S_s)	8"	4 3/4"	6 1/2"
Area of Sampling Sector ($A_s = \frac{S_s r_s}{2}$)	56 in^2	31.85 in^2	45.5 in^2
Radius of paper (r_p)	14 1/4"	13 1/4"	14 1/4"
Area of paper (S_p)	8"	5 1/4"	6 1/2"
Area of paper ($Ap = \frac{S_p r_p}{2}$)	57 in^2	34.8 in^2	46.3 in^2
Wt of Particles and Ash	4.4 mg	2.7 mg	3.6 mg
Wt of Paper Ash (Apx .0772 mg/in^2)	279.7 mg	232.7 mg	317.0 mg
Wt of particles	275.3 mg	230.0 mg	313.4 mg
% of total paper ($\frac{AS}{684}$)	8.19%	4.66%	6.65%
Wt of particles on total paper	3.36 gm	4.94 gm	4.72 gm
Wt of particles mounted for beta counting	24.4 mg	30.8 mg	40.7 mg
Reserve sample	248.4 mg	197.8 mg	272.1 mg

Separation of Particles by Size

The following apparatus was constructed in order to obtain homogeneous mixing.

Blades of Propeller

Top

Side

Blade pitch set at 45 degrees to vertical and each of the four blades is set at 90 degrees rotation with respect to the nearest neighboring set of blades.

Stirring Motor

Stirring paddle with blades pitched to push particles toward top of cylinder

500 ml graduated cylinder
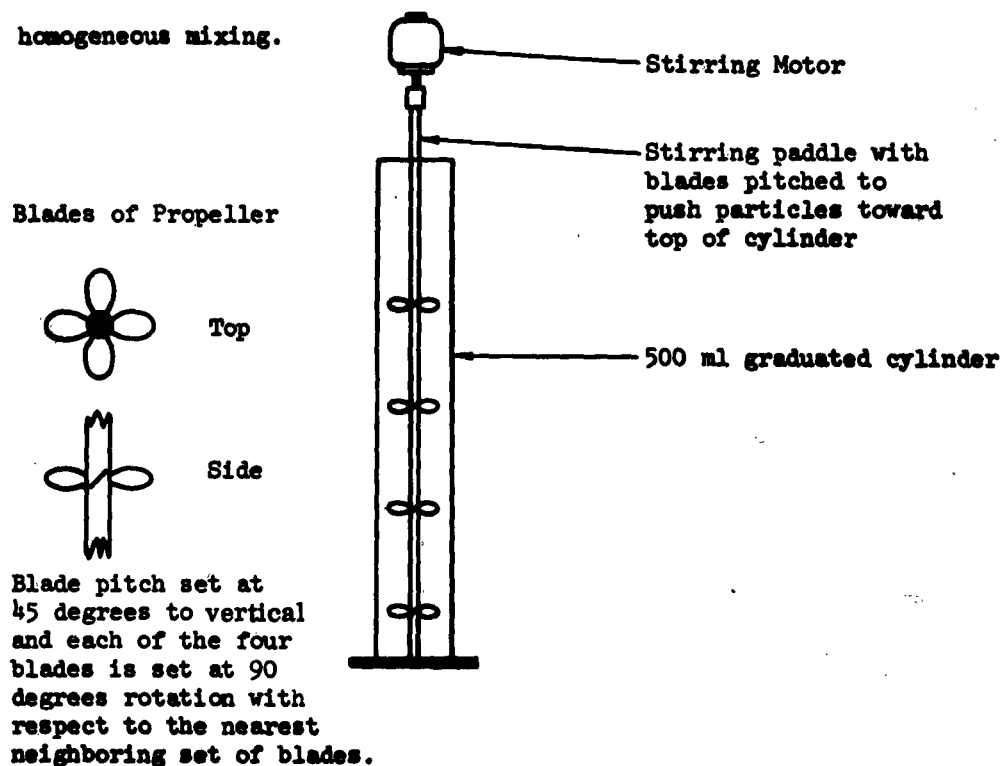
The particles which remained after the ashing were slurried in benzene and transferred to the 500-ml graduated cylinder. Benzene (reagent grade) was added to bring the liquid up to the 500-ml mark. The stirring paddle was inserted into the solution and the solution was stirred for thirty minutes. The paddle was then removed and rinsed with a few milliliters

and the remaining 3/4 of the sample was reserved for gamma
spectra analysis. There were a total of 28 samples produced
by this method.

Microscope Sizing of Particles.

One quarter of the filtered particles was placed in a test
tube and about two ml of a dilute collodion solution (1 part
collodion; 10 parts ethyl alcohol; 10 parts ethyl ether)
was added to slurry the particles. The slurry was then transferred
to a glass plate and allowed to evaporate. The resultant layer
was very thin and allowed two-dimensional measurement of the
particles.

The apparatus used was a Bausch and Lomb microscope with
12.5 power eyepieces and 8X, 10X, 20X, and 40X lenses giving
total magnifications of 100X, 125X, 250X, and 500X. The
measuring device was a variable hairline eyepiece that
appeared as such.
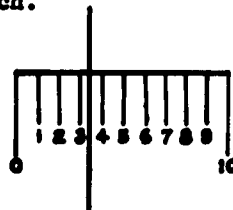
Each time the dial on the right of the eyepiece rotated
one revolution, the hairline moved one division on the
scale. The dial was graduated in one hundred divisions.

105

The scales were calibrated by placing a standard plate graduated in 0.1 mm and 0.01 mm under the microscope and finding the number of divisions on the eyepiece scale corresponding to 0.01 mm.

The following calibrations were determined.

100X	1.03 divisions/micron
125X	1.27 divisions/micron
250X	2.70 divisions/micron
500X	5.27 divisions/micron

The lower limit of measurement was around 5 divisions on each of the scales and the precision for each measurement was 2 divisions.

The plates containing the particles were placed on the stage of the microscope and the stage was moved to find an area of significant concentration of particles. The field of measurement was a rectangle bordered on the sides by the #0 and #10 lines and on the top and bottom by the ends of the shortest lines (e.g., line No. 4). The stage was then moved vertically to the next field. This was continued until a suitable number of measurements had been obtained.

The measurements were all made horizontally and measured only the horizontal width as the particle was lying. The following diagrams will show the distance measured for

SECRET

various types of particles. This distance is from point A
to point B.
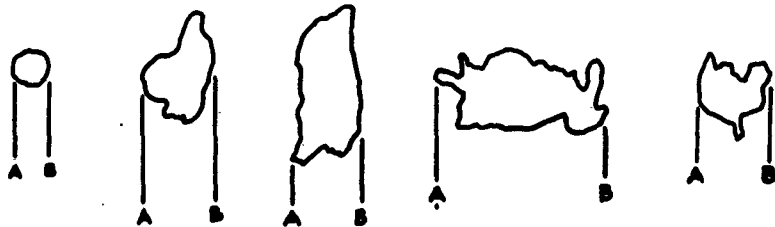
The distance from A to B was found by taking the difference
between the two readings on the scale mounted on the eyepiece.
The measurements were recorded as divisions and classified
by frequency occurrence for each size.

In order to obtain a statistical distribution of the
number of small particles with relation to the number of large
particles, glass plates of particles from unfractionated
portions of Samples 827-L-1-1 and 842-L-2 were measured at
magnifications of 5.27, 2.70, and 1.03 divisions per micron.
The conversion factor of the areas observed is expressed by:

$$\frac{(5.27)^2}{(.103)^2} = 26.2 \text{ and } \frac{(2.70)^2}{(1.03)^2} = 6.88$$

107

of benzene and the solution was allowed to settle for 120
minutes. The top 400 ml of the 500 ml of liquid was then
carefully siphoned off and filtered on a filter tower through
Whatman # 42 7/8-inch diameter filter paper. (On a total sample
slurried in benzene and filtered by this method, no appreciable
radioactivity was found when the filtrate was evaporated
to dryness on a platinum disc.)

The above procedure was then repeated in order to obtain
the other fractions. This procedure produced seven size fractions
as follows:

Stirring Time	Settling Time	Nomenclature of Fraction
30 minutes	120 minutes	120
30 minutes	60 minutes	60
30 minutes	30 minutes	30
5 minutes	15 minutes	15
5 minutes	5 minutes	5
5 minutes	1 minute	1
None	None	Residue

This procedure was accomplished on samples from 14,000 (Figure B.1);
11,000; 12 to 14,000 and 9,500 feet. Each of the filter papers
containing the particles was sliced with a scalpel into two
fractions, one-fourth of the samples being used for particle sizing.

If the particle size frequency for all of the particles measured at 5.27 div/μ magnification is multiplied by 26.2, it will bring both sets of data into comparison for the total particle size picture.

The heavier fractions from the various altitudes contained spheres ranging in diameter from 20 microns to 150 microns. Some of these spheres had cracked surfaces and others appeared to be completely smooth. Some of the spheres had been broken, possibly in the mixing of the samples. Some of the heavier fractions and the unfractionated samples were measured for spheres only. Each fraction was photographed. Many of these photographs show clearly the presence of the previously described spheres.

Following is a listing of the number of particles sized from each of the fractions.

		All Particles		Spheres Only	
		Number Sized	Magnifi- cation	Number Sized	Magnifi- cation
9.5K	Residue	400	100X	100	100X
9.5K	1 Minute	440	100X	-	-
9.5K	5 Minute	360	100X	-	-
9.5K	15 Minute	300	250X	-	-
9.5K	30 Minute	260	250X	-	-

109

		All Particles		Spheres Only	
		Number Sized	Magnifi- cation	Number Sized	Magnifi- cation
9.5K	60 Minute	240	500X	–	–
9.5K	120 Minute	200	500X	–	–
14K	Residue	400	100X	100	100X
14K	1 Minute	400	125X	60	100X
14K	5 Minute	300	100X	–	–
14K	15 Minute	400	500X	–	–
14K	30 Minute	280	250X	–	–
14K	60 Minute	432	500X	–	–
14K	120 Minute	320	500X	–	–
14K	Unfractionated	285	100X	60	100X
14K	Unfractionated	311	250X	–	–
14K	Unfractionated	360	500X	–	–
11K	Unfractionated	112	100X	233	100X
11K	Unfractionated	253	250X	–	–
11K	Unfractionated	360	500X	–	–

120 Minute   19μ/div   60 Minute   19μ/div

15 Minute   37μ/div   5 Minute   37μ/div

Residue   97μ/div
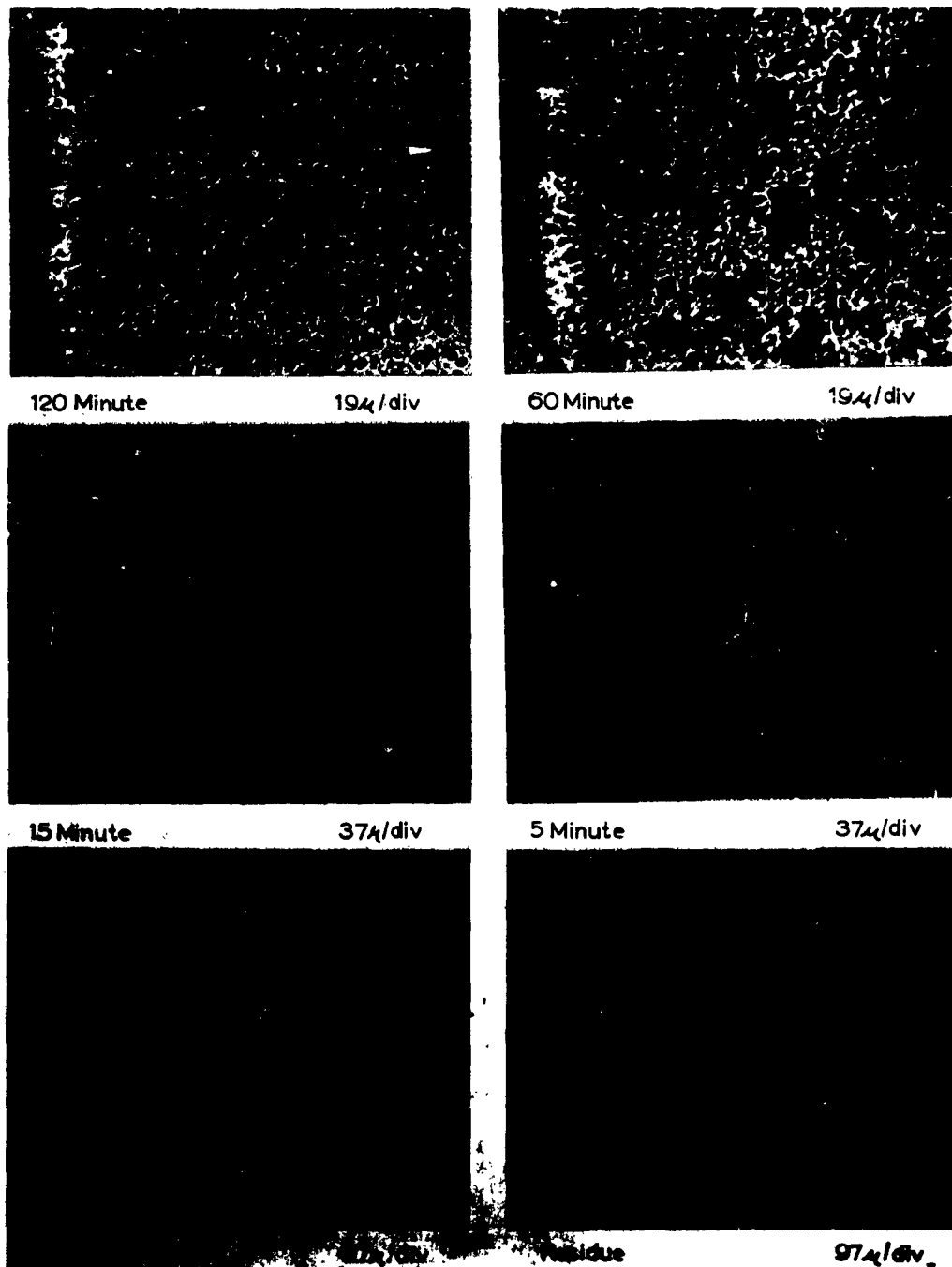
Figure B. 1   Photomicrographs of 14,000-foot fractionated samples.

111

SECRET

Appendix C

CALCULATED DISTRIBUTION FUNCTIONS FOR BENZENE EXPERIMENT

$$\overline{D}_g = .50 \quad D \text{ Cut-Off-49}\mu$$

Fraction	2.00	2.25	2.50	2.75	3.00
120m	50.26	38.82	27.44	17.89	10.97
60m	16.91	15.01	12.38	9.49	6.88
30m	8.29	8.91	8.82	8.02	6.77
15m	5.93	7.46	8.47	8.70	8.23
5m	6.75	9.79	12.70	14.83	15.90
1m	7.68	12.77	19.01	25.47	31.33
residue	4.15	7.20	11.17	15.57	19.88

$$\overline{D}_g = 1.00 \quad D \text{ Cut-Off-49}\mu$$

	2.00	2.25	2.50	2.75	3.00
120m	41.41	31.83	22.78	15.26	9.68
60m	17.07	14.77	12.01	9.20	6.69
30m	9.80	9.87	9.31	8.21	6.84
15m	7.53	8.63	9.17	9.05	8.38
5m	8.76	11.45	13.82	15.46	16.20
1m	10.00	14.97	20.70	26.55	31.92
residue	5.39	8.44	12.17	16.24	20.26

$$\overline{D}_g = 2.00 \quad D \text{ Cut-Off-49}\mu$$

	2.00	2.25	2.50	2.75	3.00
120m	29.49	22.64	16.45	11.35	7.48
60m	16.91	14.21	11.38	8.67	6.34
30m	11.79	11.06	9.95	8.49	6.94
15m	9.75	10.21	10.14	9.57	8.62
5m	11.59	13.72	15.40	16.42	16.72
1m	13.28	17.96	23.09	28.21	32.95
residue	7.23	10.18	13.60	17.27	20.92

$$\overline{D}_g = 3.00 \quad D \text{ Cut-Off-49}\mu$$

	2.00	2.25	2.50	2.75	3.00
120m	20.74	15.94	11.71	8.25	5.58
60m	16.21	13.39	10.62	8.09	5.94
30m	13.18	11.93	10.37	8.68	7.00
15m	11.48	11.41	10.89	10.00	8.84
5m	13.85	15.50	16.66	17.24	17.19
1m	15.91	20.33	25.00	29.62	33.91
residue	10.23	12.66	15.55	18.77	21.86

$$\overline{D} = .50 \quad D \text{ Cut-Off } 76\mu$$

Fraction	2.00	2.25	2.50	2.75	3.00
120m	48.18	35.64	23.57	14.10	7.84
60m	16.21	13.78	10.63	7.48	4.91
30m	7.95	8.18	7.58	6.32	4.84
15m	5.69	6.85	7.28	6.86	5.88
5m	6.48	8.99	10.91	11.70	11.36
1m	8.18	13.30	18.97	23.95	27.49
residue	7.29	13.23	21.04	29.56	37.65

$$\overline{D} = 1.00 \quad D \text{ Cut-Off } 76\mu$$

120m	39.21	28.81	19.33	11.92	6.87
60m	16.16	13.37	10.19	7.19	4.76
30m	9.28	8.94	7.90	6.42	4.86
15m	7.13	7.81	7.78	7.07	5.95
5m	8.30	10.37	11.73	12.09	11.51
1m	10.51	15.37	20.41	24.75	27.87
residue	9.38	15.30	22.64	30.54	38.16

$$\overline{D} = 2.00 \quad D \text{ Cut-Off } 76\mu$$

120m	27.44	20.11	13.72	8.76	5.27
60m	15.73	12.62	9.49	6.69	4.46
30m	10.97	9.86	8.30	6.55	4.88
15m	9.08	9.06	8.46	7.38	6.07
5m	10.79	12.19	12.84	12.66	11.77
1m	13.72	18.11	22.37	25.94	28.49
residue	12.30	18.06	24.84	32.03	39.04

$$\overline{D} = 3.00 \quad D \text{ Cut-Off } 76\mu$$

120m	19.04	13.95	9.64	6.29	3.89
60m	14.88	11.73	8.74	6.16	4.14
30m	12.10	10.44	8.53	6.62	4.89
15m	10.54	9.99	8.96	7.62	6.17
5m	12.72	13.57	13.71	13.14	12.00
1m	16.22	20.19	23.90	26.94	29.07
residue	15.99	21.14	27.19	33.65	40.05

113

$$\overline{D} = .50 \quad D \text{ Cut-Off-137}\mu$$

Fraction	2.00	2.25	2.50	2.75	3.00
120m	45.94	32.10	19.39	10.32	5.00
60m	15.46	12.42	8.75	5.48	3.14
30m	7.58	7.37	6.23	4.62	3.09
15m	5.43	6.17	5.99	5.02	3.76
5m	6.18	8.09	8.98	8.55	7.25
1m	7.80	11.98	15.62	17.51	17.56
residue	11.60	21.84	35.02	48.50	60.18

$$\overline{D} = 1.00 \quad D \text{ Cut-Off-137}\mu$$

Fraction	2.00	2.25	2.50	2.75	3.00
120m	36.90	25.57	15.70	8.64	4.37
60m	15.21	11.87	8.28	5.21	3.03
30m	8.74	7.93	6.42	4.65	3.09
15m	6.71	6.93	6.32	5.12	3.78
5m	7.81	9.20	9.52	8.75	7.31
1m	9.89	13.64	16.57	17.94	17.71
residue	14.73	24.86	37.18	49.67	60.70

$$\overline{D} = 2.00 \quad D \text{ Cut-Off-137}\mu$$

Fraction	2.00	2.25	2.50	2.75	3.00
120m	25.37	17.49	10.94	6.26	3.32
60m	14.55	10.98	7.56	4.78	2.82
30m	10.15	8.58	6.62	4.68	3.08
15m	8.39	7.88	6.74	5.27	3.83
5m	9.97	10.60	10.25	9.05	7.42
1m	12.68	15.74	17.85	18.55	17.96
residue	18.95	28.74	40.05	51.39	61.57

$$\overline{D} = 3.00 \quad D \text{ Cut-Off-137}\mu$$

Fraction	2.00	2.25	2.50	2.75	3.00
120m	17.36	11.96	7.58	4.45	2.44
60m	13.57	10.05	6.87	4.36	2.59
30m	11.03	8.95	6.71	4.67	3.06
15m	9.61	8.56	7.05	5.38	3.86
5m	11.59	11.62	10.78	9.29	7.51
1m	14.79	17.30	18.80	19.05	18.19
residue	23.40	32.44	42.71	53.07	62.49

114

SECRET

$$\overline{D} = .50 \text{ D Cut-Off-120}\mu$$

Fraction	2.00	2.25	2.50	2.75	3.00
120m	46.40	30.84	20.25	11.06	5.54
60m	15.61	12.70	9.13	5.87	3.47
30m	7.66	7.54	6.51	4.96	3.42
15m	5.48	6.31	6.25	5.38	4.16
5m	6.24	8.28	9.38	9.17	8.02
1m	7.88	12.26	16.30	18.78	19.41
residue	10.72	20.06	32.16	44.77	55.97

$$\overline{D} = 1.00 \quad \text{D Cut-Off-120}\mu$$

	2.00	2.25	2.50	2.75	3.00
120m	37.36	26.23	16.43	9.28	4.84
60m	15.40	12.18	8.67	5.60	3.35
30m	8.85	8.13	6.71	5.00	3.42
15m	6.80	7.11	6.62	5.50	4.19
5m	7.91	9.44	9.97	9.41	8.10
1m	10.02	13.99	17.35	19.27	19.60
residue	13.65	22.90	34.24	45.93	56.50

$$\overline{D} = 2.00 \quad \text{D Cut-Off-120}\mu$$

	2.00	2.25	2.50	2.75	3.00
120m	25.78	18.02	11.50	6.74	3.68
60m	14.78	11.31	7.95	5.15	3.12
30m	10.31	8.84	6.96	5.05	3.41
15m	8.52	8.12	7.08	5.68	4.24
5m	10.14	10.92	10.77	9.75	8.23
1m	12.89	16.22	18.75	19.99	19.91
residue	17.62	26.59	37.02	47.65	57.40

$$\overline{D} = 3.00 \quad \text{D Cut-Off-120}\mu$$

	2.00	2.25	2.50	2.75	3.00
120m	17.69	12.36	7.99	4.80	2.71
60m	13.83	10.38	7.24	4.71	2.88
30m	11.24	9.25	7.07	5.05	3.40
15m	9.80	8.85	7.43	5.82	4.29
5m	11.82	12.02	11.36	10.02	8.34
1m	15.07	17.85	19.80	20.57	20.19
residue	21.94	30.20	39.65	49.34	58.37

Appendix D

ELECTRON MICROPROBE ANALYSIS

Two hundred and fifty Johnie Boy particles have been
analyzed by an Applied Research electron microprobe. Elemental
analysis within the limits of the probe was performed on
particles sampled from different heights in the atmosphere.
Ratios of the elements versus particle size were calculated for
the Johnie Boy particles. Electron backscatter displays
were used as a criterion for determining the size of the
particles (see Figures D.3a, D.3c, and D.3d), as well as means
for positioning the analyzing beam.

OPERATING CONDITIONS AND PROCEDURES

Particle Sizes. Particle sizes determined by the electron
backscatter displays were validated by a calibrated, standard,
copper-silver grid whose wire mesh diameters were determined
by Applied Research Laboratories. On a 360-micron sweep at
a 30-kv accelerating potential the electron beam covers an
area of 129,600 square microns. Under these conditions, at
an electronic magnification of 1X (optical equivalent 222X)
the dominant copper grid wire has a diameter of thirty microns
edge to edge. From the copper wire grid backscatter representa-
tion on the oscilloscope, it was determined that each small
gradient represented 5 microns in length.

116

Particle Analysis. An electron beam accelerating voltage
of 30 kv was used, and a sample current of 0.05 microamps
was maintained throughout the analysis. A beam spot size of
approximately 1 micron was used. The particles from Johnie
Boy were mounted on highly polished beryllium rods and placed
in a specimen holder. These particles were then positioned
inside the probe. A spot scan from edge to edge of the particle
was used for the analysis. The intensity versus wavelength data
were recorded and subsequently used to determine a relative
weight percent of the elements present.

Standardization. The Johnie Boy particles were calibrated
against eighteeen stainless steel microspheres. The analysis
of the microspheres was carried out at 30 kv and 0.05 microamps
sample current. However, a somewhat different 4-inch LiF detector
voltage setting was used than for the Johnie Boy particles.
The results of the microspheres analyses are listed in Table D.1.
The ratios of Cr/Fe and Ni/Fe in the microspheres are plotted
in Figure D.2.

Our analysis of these spheres agreed with independent
microprobe data from Tracerlab on the same controlled sample
batch. The compositions of the stainless steel microspheres
were independent of particle size.

117

SECRET

The next step was the recalibration and calculation
of the relative elemental percentages of the Johnie Boy
particles with respect to the same 4-inch LiF detector setting as
was used for the stainless steel microspheres. The recorder
unit scale readings were adjusted to give readings equivalent
to those which would have been obtained had the X-ray
detector settings been the same for the Johnie Boy particles
and the stainless steel microspheres.

Elemental ratios have been plotted for the Johnie Boy
particles (see Figure D.1). The final relative mean average
composition for the Johnie Boy particles was calculated taking
into account corrections for absorbance and atomic number.
These final calculations are listed in Table D.2.

The formula used for the relative mean average composition
of the Johnie Boy particles was the following:

$$\overline{X}'_{(n)} \cdot A_{(n)} \cdot B_{(n)} = \overline{X}'_{(n)}$$

where $\overline{X}'_{(n)}$ = Initial relative mean average composition
for element (n).

$A_{(n)}$ = Absorbance correction factor for element (n).

$B_{(n)}$ = Atomic number correction factor for element (n).

$\overline{X}'_{(n)}$ = Final relative mean average composition for element (n).

RESULTS AND DISCUSSION

The following elements were scanned for and were not found to be present in the Johnie Boy spherical metallic oxide particles within the detectable limits of the probe: Al, U, Ti, Sn, Pb, Ta, Rb, W, Mg, Cu, Ag, Au.

The relative mean average composition of the metallic oxide particulates, which indeed constituted the majority under investigation was 64.9% Fe, 2.0% Mn, 19.4% Cr, 14.4% Ni (see Figure D.1). Some thirty metallic particles contained zinc and six of these thirty particles contained traces of cobalt. It was found that the analytical results were independent of the particle size.

Many of the Johnie Boy metallic particles were elliptodial or spherical in shape, some were irregular in shape (Figures D.3a, D.3c) as compared to Figure D.3d, an electron backscatter display of spherical stainless steel microspheres.

Most of the Johnie Boy particles contained iron, with the elements Mn, Cr, Ni, Zn being present. All showed a tendency to be enriched relative to iron as the particle size increased (see Figure D.1).

119

SECRET

TABLE D.1   316 STAINLESS STEEL MICROSPHERES

No.	Size μ	Fe	Cr	Ni
1	55	63.5	20.0	13.5
2	45	62.5	21.5	13.0
3	30	62.0	20.5	14.0
4	45	62.0	22.0	13.0
5	50	63.0	21.5	12.5
6	15	62.5	20.5	13.5
7	25	62.0	21.5	13.0
8	20	62.0	20.5	13.0
9	25	62.0	21.0	13.5
10	20	63.0	22.0	13.0
11	35	62.5	21.5	13.5
12	45	62.0	22.0	13.0
13	30	62.0	21.0	13.5
14	55	63.0	20.0	13.0
15	40	62.5	21.5	13.0
16	55	62.5	21.0	13.5
17	40	62.0	20.5	14.0
18	35	63.0	21.5	13.0

Mn, for all particles 1.5%

TABLE D.2   CORRECTION FACTORS FOR ELECTRON
MICROPROBE ANALYSES

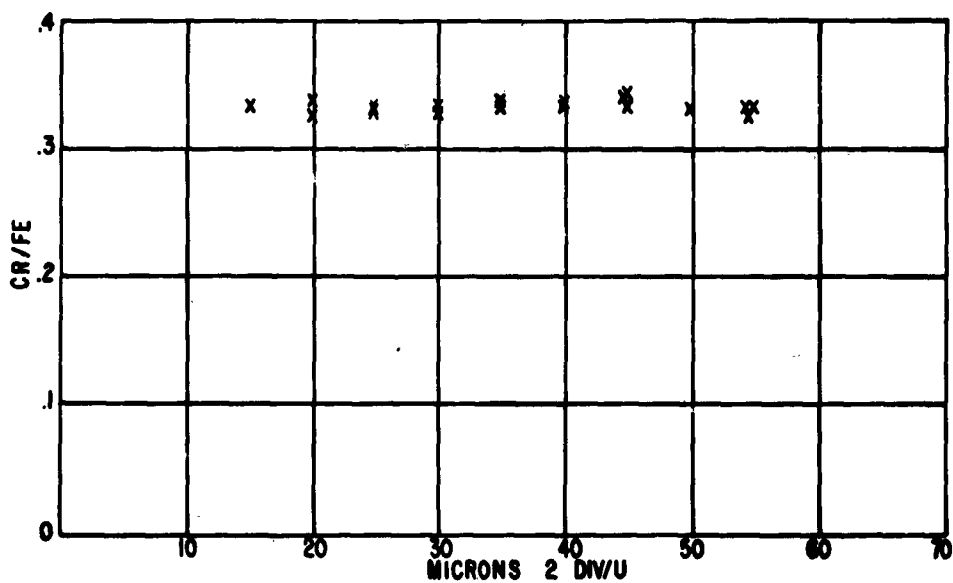| (n)	$\vec{X}'_{(n)}$	$A_{(n)}$	$B_{(n)}$	$\vec{X}'_{(n)}$
Fe	66.0	1.00	.984	64.9
Ni	13.2	1.10	.992	14.4
Mn	2.2	1.00	.910	2.0
Cr	17.5	1.15	.965	19.4

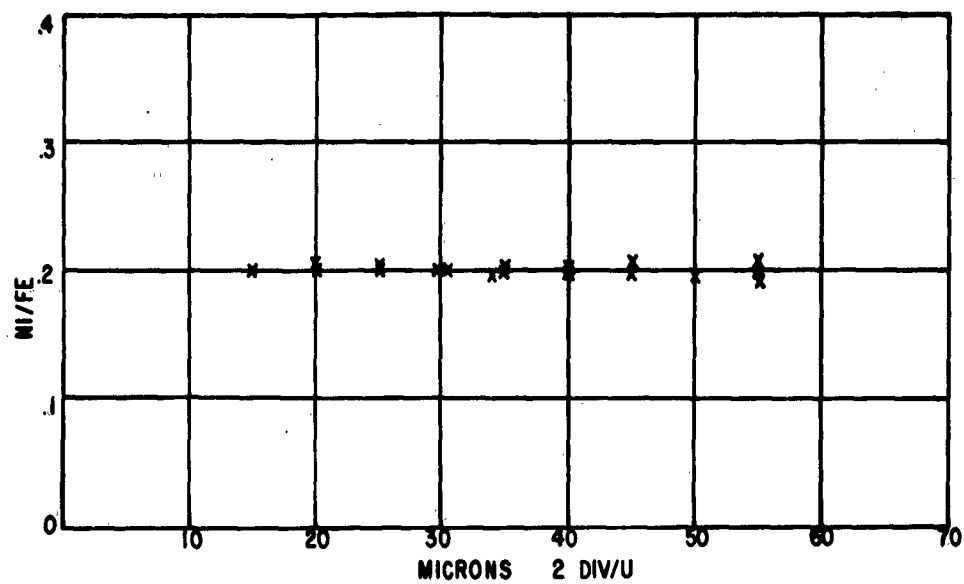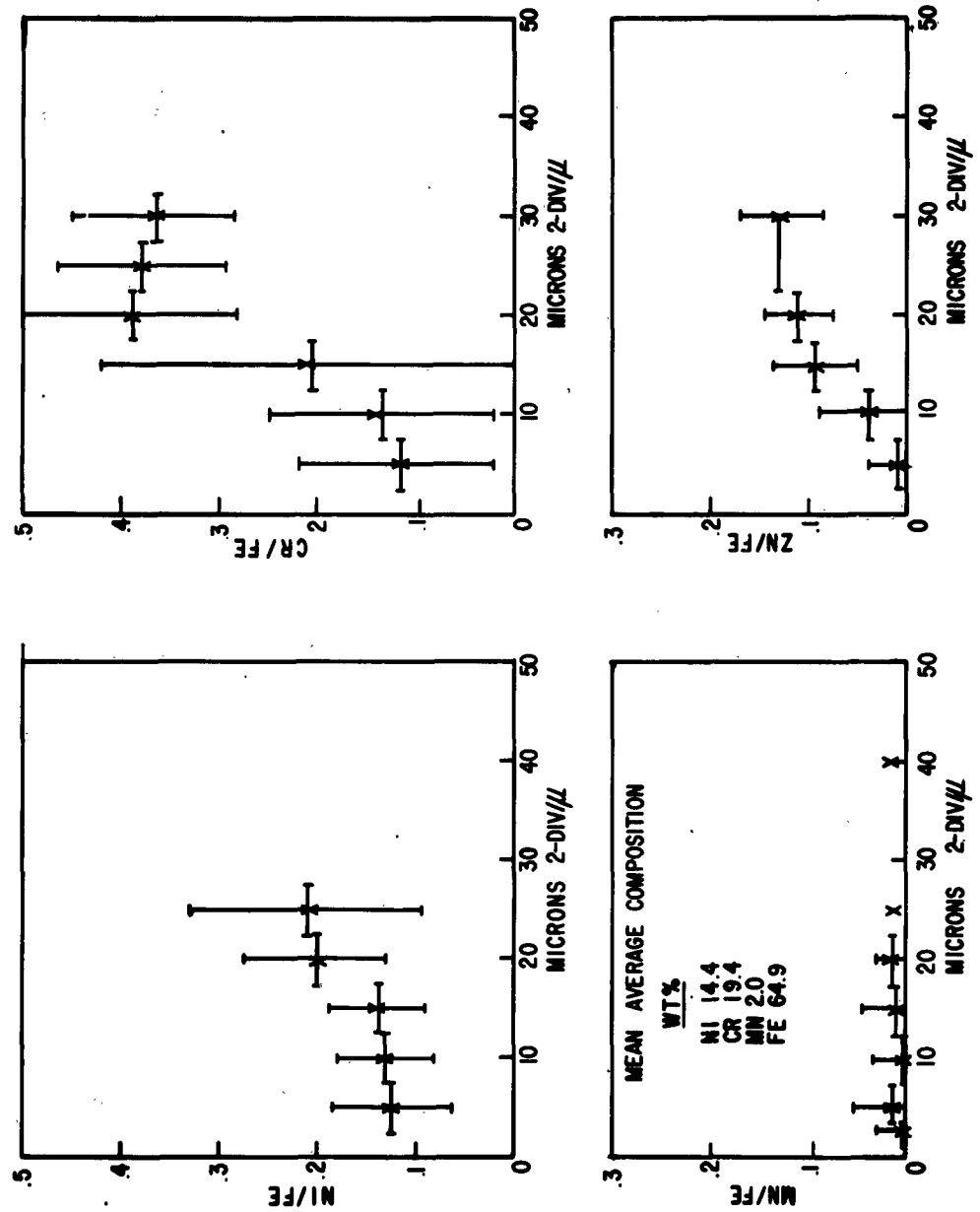Figure D.1 316 stainless steel microspheres.

121

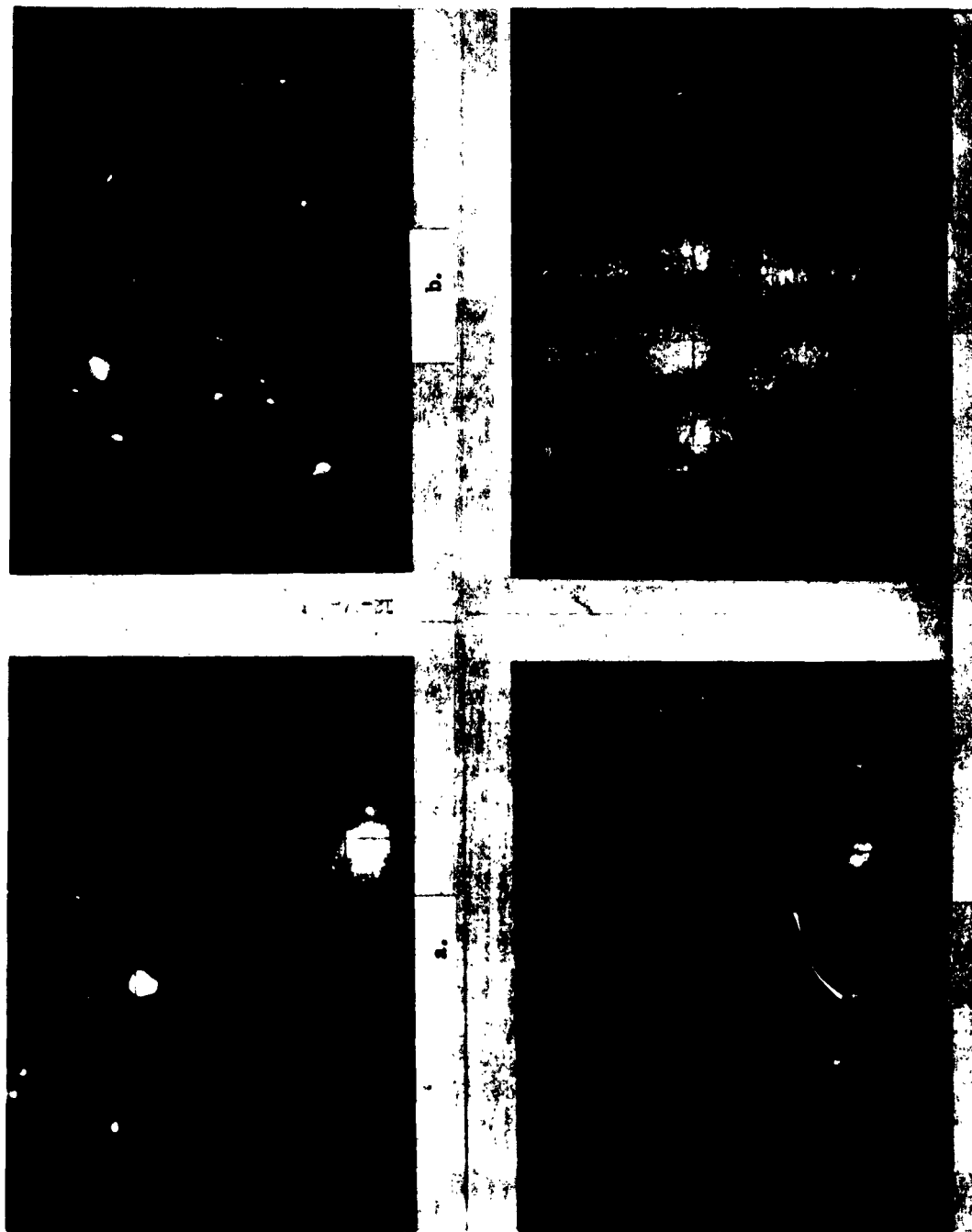Figure D.2 Microprobe analysis.

122

Figure D.3 Photographs of Johnie Boy metallic particles.

123

REFERENCES

1. E.C. Freiling; "Radionuclide Fractionation of Bomb Debris"; Science 133, 3469, June 1961; Unclassified.

2. E.C. Freiling; "Theoretical Basis for Logarithmic Correlations of Fractionated Radionuclide Composition"; Science 139, 3539, March 1963; Unclassified.

3. P.C. Stevenson; "Correlation of Fractionation Phenomena in the Tewa Event of Operation Redwing, Suggestion for the Control of Fractionation"; UCRL-5027, University of California, Livermore Radiation Lab.; November 1957; Secret Restricted Data.

4. I.J. Russell; "Specific Activity and Particle Size Relationships of Airburst Debris Particles"; Air Force Weapons Laboratory Unpublished Notes; 1964; Secret Restricted Data.

5. "Compilation of Radioactive Fallout Prediction Systems"; Volume 3, Working Papers compiled for USNRDL-DASA Fallout Symposium Project; September 1962.

6. M.J. Schumchyk and E.H. Bouton; "Fallout Studies"; Project 2.5.1, Operation Teapot; WT-1119; July 1958; Chemical and Radiological Laboratories, Army Chemical Center, Maryland; Unclassified.

7. "Operation Jangle, Radiochemical Measurements and Sampling Techniques"; WT-373, June 1952; Confidential.

8. "Particle Studies"; Operation Jangle; WT-371, July 1952; Armed Forces Special Weapons Project, Washington, D.C.; Secret Restricted Data.

9. D.E. Clark, F.K. Kawahara, and W.C. Cobbin; "Fallout Sampling and Analysis"; Operation Sun Beam, Project 2.9, POR-2289; October 1963; Naval Radiological Defense Laboratory, San Francisco, California; Secret Restricted Data.

10. K. Steward; "The Condensation of a Vapor to an Assembly of Droplets or Particles"; Trans. Faraday Society, Vol. 52; 1956; Unclassified.

11. E.H. Bouton; "Radiological Survey"; Operation Sun Beam, Project 2.8, POR-2266; September 1962; U.S. Army Chemical Corps, Nuclear Defense Laboratory, Army Chemical Center, Maryland.

12. R.C. Bolles and N.E. Ballou; "Calculated Activities and Abundances of U^{235} Fission Products"; USNRDL Report; August 1956.

124

DISTRIBUTION

Military Distribution Category 26

ARMY ACTIVITIES

1 CHIEF OF R & D DA
2 AC OF S INTELLIGENCE DA
3 ASST.C OF S FORCE DEV. ATTN CHR-OPNS
4 CHIEF OF ENGINEERS DA
5- 6 ARMY MATERIAL COMMAND
7 CHIEF SIGNAL OFFICER DA
8 CHIEF OF TRANSPORTATION DA
9- 10 THE SURGEON GENERAL DA
11- 12 U S ARMY COMBAT DEVELOPMENTS COMMAND
13 U S ARMY CDC NUCLEAR GROUP
14 U S ARMY ARTILLERY BOARD
15 U S ARMY AIR DEFENSE BOARD
16 U S ARMY AVIATION BOARD
17 ARMY WAR COLLEGE
18 U S ARMY AIR DEFENSE SCHOOL
19 U S ARMY CDC ARMOR AGENCY
20 U S ARMY CDC ARTILLERY AGENCY
21 U S ARMY CDC INFANTRY AGENCY
22 U S MILITARY ACADEMY
23 QUARTERMASTER SCHOOL U S ARMY
24 U S ARMY ORDNANCE & GUIDED MISSILE SCHOOL
25 U S ARMY CDC CBR AGENCY
26 U S ARMY CBR WEAPONS SCHOOL
27 U S ARMY SIGNAL SCHOOL
28 U S ARMY TRANSPORTATION SCHOOL
29 ENGINEER SCHOOL
30 MEDICAL FIELD SERVICE SCHOOL
31 U S ARMY NUCLEAR MEDICAL RESEARCH DET EUROPE
32 ARMED FORCES INSTITUTE OF PATH
33 WALTER REED ARMY INST OF RES
34 GENERAL SUPPLIES RESEARCH & ENGINEERING LAB
35 ENGINEER RESEARCH & DEV LAB
36 WATERWAYS EXPERIMENT STATION
37 DIAMOND ORDNANCE FUZE LABORATORY
38- 39 BALLISTIC RESEARCH LABORATORY
40 ARMY MATERIALS RESEARCH AGENCY
41 U S ARMY MOBILITY COMMAND
42 U S ARMY MUNITIONS COMMAND
43 ELECTRONICS COMMAND
44 U S ARMY ELECTRONIC PROVING GROUND
45- 46 U S ARMY ELECTRONIC R & D LABORATORY
47- 48 U S ARMY CDC COMBAT SERVICE SUPPORT GROUP
49 THE RESEARCH & ANALYSIS CORP
50 WHITE SANDS SIGNAL SUPPORT AGENCY
51- 52 U S ARMY NUCLEAR DEFENSE LABORATORY
53 U S ARMY CDC AIR DEFENSE AGENCY
54 U S ARMY CORPS OF ENG NUCLEAR CRATERING
55 UNITED STATES CONTINENTAL ARMY COMMAND
56 CHIEF OF R&D DEPARTMENT OF THE ARMY
57 U S ARMY CDC COMBINED ARMS GROUP
58 US ARMY ENGR.RES. & ENGR.LABS.

NAVY ACTIVITIES

59- 60 CHIEF OF NAVAL OPERATIONS OP03EG
61 CHIEF OF NAVAL OPERATIONS OP-09B5
62 CHIEF OF NAVAL OPERATIONS OP-75
63 CHIEF OF NAVAL OPERATIONS OP-92262
64 CHIEF OF NAVAL PERSONNEL
65 CHIEF OF NAVAL OPERATIONS OP-94
66 CHIEF OF NAVAL OPERATIONS OP-922F2
67- 69 CHIEF BUREAU OF NAVAL WEAPONS DLI-3
70 CHIEF BUREAU OF MEDICINE & SURGERY CODE 74
71 CHIEF BUREAU OF SHIPS CODE 423
72 CHIEF BUREAU OF SHIPS CODE 362
73 CHIEF BUREAU OF YARDS & DOCKS CODE 74
74 DIR. US NAVAL RESEARCH LAB.
75- 76 U S NAVAL ORDNANCE LABORATORY
77 MATERIAL LABORATORY CODE 900
78 NAVY ELECTRONICS LABORATORY
79- 82 U S NAVAL RADIOLOGICAL DEFENSE LAB
83 U S NAVAL CIVIL ENGINEERING LABORATORY
84 U S NAVAL ACADEMY
85 U S NAVAL SCHOOLS COMMAND U S NAVAL STATION
86 U S NAVAL WAR COLLEGE

87 U S NAVAL POSTGRADUATE SCHOOL
88 U S NAVAL SCHOOL CEC OFFICERS
89 U S NAVAL DAMAGE CONTROL TNG CENTER ABC
90 U S NAVAL MEDICAL RESEARCH INSTITUTE
91 U S NAVAL ORDNANCE TEST STATION
92 DAVID W TAYLOR MODEL BASIN
93 U S NAVAL SUPPLY R&D FACILITY
94- 97 U S MARINE CORPS CODE A03H

AIR FORCE ACTIVITIES

98- 99 HQ USAF AFTAC-TD
100 HQ USAF AFRDPF
101 HQ USAF AFXPDG
102 HQ USAF AFOCEKA
103 HQ USAF AFGOA
104-108 HQ USAF AFNINDE
109 AC OF S INTELLIGENCE HQ USAFE
110 BALLISTIC SYSTEMS DIVISION
111 HQ USAF AFMSPAA
112 TACTICAL AIR COMMAND
113 ALASKAN AIR COMMAND
114 AIR DEFENSE COMMAND
115 AIR FORCE SYSTEMS COMMAND
116 PACIFIC AIR FORCES
117-118 AF CAMBRIDGE RESEARCH CENTER
119-123 AFWL WLL-3 KIRTLAND AFB
124-125 AIR UNIVERSITY LIBRARY
126 LOWRY TECH.TNG.CEN. TS-W
127 SCHOOL OF AVIATION MEDICINE
128-129 AERONAUTICAL SYSTEMS DIVISION
130-131 USAF PROJECT RAND
132 AIR TECHNICAL INTELLIGENCE CENTER
133 HQ USAF AFORQ
134 HQ USAF AFXPDK

OTHER DEPARTMENT OF DEFENSE ACTIVITIES

135 DIRECTOR OF DEFENSE RESEARCH AND ENGINEERING
136 ASST TO THE SECRETARY OF DEFENSE ATOMIC ENERGY
137 MILITARY LIAISON COMMITTEE
138 WEAPONS SYSTEM EVALUATION GROUP
139 ASST SECRETARY OF DEFENSE INSTALLATION & LOGISTICS
140 INDUSTRIAL COLLEGE OF THE ARMED FORCES
141 ARMED FORCES STAFF COLLEGE
142-145 DEFENSE ATOMIC SUPPORT AGENCY
146 FIELD COMMAND DASA
147 FIELD COMMAND DASA FCTG
148-149 WEAPONS TEST DIV.,DASA,SANDIA,WTWT-TI
150 U S COAST GUARD
151 JOINT TASK FORCE-8
152 COMMANDER-IN-CHIEF PACIFIC
153 COMMANDER-IN-CHIEF ATLANTIC FLEET
154 STRATEGIC AIR COMMAND
155 CINCONAD
156-158 ASST SECRETARY OF DEFENSE CIVIL DEFENSE
159 DIR.DEFENSE INTELLIGENCE AGENCY
160-179 DEFENSE DOCUMENTATION CENTER

FOR CIVILIAN DISTR CAT. B 3

180 ISOTOPES WESTWOOD NEW JERSEY
181 STANFORD RESEARCH INST. ATTN RUBIN
182 RAND CORP SANTA MONICA CALIF ATTN TECH.LIBRARY
183 US WEATHER BUREAU WASHINGTON ATTN FERBER
184 SPERRY RAND CORP LONG ISLAND N Y
185 GENERAL ELCTRIC CO DEF.ELEC.DIV.

ATOMIC ENERGY COMMISSION ACTIVITIES

186-188 AEC WASHINGTON TECH LIBRARY
189-190 LOS ALAMOS SCIENTIFIC LAB
191-195 SANDIA CORPORATION
196-205 LAWRENCE RADIATION LAB LIVERMORE
206 NEVADA OPERATIONS OFFICE,LAS VEGAS
207 DTIE OAK RIDGE,MASTER
208-237 DTIE OAK RIDGE SURPLUS

125

SECRET

RESTRICTED DATA